The internal deformation of the Peridotite Nappe of New Caledonia: a structural study of serpentine-bearing faults and shear zones in the Koniambo Massif

Benoît Quesnel, Pierre Gautier, Michel Cathelineau, Philippe Boulvais, Clément Couteau, Maxime Drouillet

Accepted Manuscript

The internal deformation of the Peridotite Nappe of New Caledonia: a structural study of serpentine-bearing faults and shear zones in the Koniambo Massif

Benoît Quesnel, Pierre Gautier, Michel Cathelineau, Philippe Boulvais, Clément Couteau, Maxime Drouillet

PII: S0191-8141(16)30015-3

DOI: 10.1016/j.jsg.2016.02.006

Reference: SG 3309

To appear in: *Journal of Structural Geology*

Received Date: 11 January 2016

Revised Date: 17 February 2016

Accepted Date: 20 February 2016

Please cite this article as: Quesnel, B., Gautier, P., Cathelineau, M., Boulvais, P., Couteau, C., Drouillet, M., The internal deformation of the Peridotite Nappe of New Caledonia: a structural study of serpentine-bearing faults and shear zones in the Koniambo Massif, *Journal of Structural Geology* (2016), doi: 10.1016/j.jsg.2016.02.006.

The internal deformation of the Peridotite Nappe of New Caledonia: a structural study of serpentine-bearing faults and shear zones in the Koniambo Massif

Benoît Quesnel[1], Pierre Gautier[1], Michel Cathelineau[2,] Philippe Boulvais[1], Clément Couteau[3], Maxime Drouillet[3]

[1] *Université Rennes 1, CNRS, Géosciences Rennes UMR 6118, OSUR, 35042 Rennes Cedex, France, benoit.quesnel@univ-rennes1.fr; pierre.gautier@univ-rennes1.fr; philippe.boulvais@univ-rennes1.fr*

[2] *Université de Lorraine, CNRS, CREGU, GeoRessources lab., 54506 Vandoeuvre-lès-Nancy, France, michel.cathelineau@univ-lorraine.fr*

[3] *Service géologique, Koniambo Nickel SAS, 98883 Voh, Nouvelle Calédonie, mdrouillet@koniambonickel.nc*

Keywords : New Caledonia, ophiolite, serpentine, magnesite, nappe, structural analysis

Abstract

We present a structural analysis of serpentine-bearing faults and shear zones in the Koniambo Massif, one of the klippes of the Peridotite Nappe of New Caledonia. Three structural levels are recognized. The upper level is characterized by a dense network of fractures. Antigorite and polygonal serpentine form slickenfibers along fault planes with distinct kinematics. As a result, the upper level keeps the record of at least two deformation events, the first associated with the growth of antigorite (WNW-ESE extension), the second with the growth of polygonal serpentine (NW-SE compression). The lower level coincides with the 'serpentine sole' of the nappe, which consists of massive tectonic breccias overlying a layer of mylonitic serpentinites. The sole records pervasive tangential shear with top-to-SW kinematics and represents a décollement at the base of the nappe. The intermediate level is characterized by

the presence of several meters-thick conjugate shear zones accommodating NE-SW shortening. Like the sole, these shear zones involve polygonal serpentine and magnesite as the main syn-kinematic mineral phases. The shear zones likely root into the basal décollement, either along its roof or, occasionally, around its base. Compared to top-to-SW shearing along the sole, the two deformation events recorded in the upper level are older.

The three structural levels correlate well with previously recognized spatial variations in the degree of serpentinization. It is therefore tempting to consider that the intensity of serpentinization played a major role in the way deformation has been distributed across the Peridotite Nappe. However, even the least altered peridotites, in the upper level, contain so much serpentine that, according to theoretical and experimental work, they should be nearly as weak as pure serpentinite. Hence, no strong vertical gradient in strength due to variations in the degree of serpentinization is expected within the exposed part of the nappe. Our proposal is that strain localization along the serpentine sole results from the juxtaposition of the nappe, made of weak serpentinized peridotites, against the strong mafic rocks of its substratum. This interpretation is at odds with the intuitive view that would consider the nappe, made of peridotites, as stronger than its basement.

1. Introduction

Ophiolites commonly occur within orogenic belts as a result of the obduction of a piece of oceanic lithosphere upon a continental basement (Coleman, 1971; Dewey and Bird, 1971). The ultramafic rocks that constitute a large part of most ophiolitic nappes generally display evidence for pronounced fluid-rock interactions in the form of a spatially uneven development of serpentinization. Due to their low strength in comparison to peridotites (e.g., Escartín et al., 2001), serpentinites have the capacity to promote strain localization and greatly influence the style of deformation on the lithosphere scale (e.g., Hirth and Guillot, 2013). Several types of serpentine may be identified in a single ophiolite, which raises the question of their relative

chronology and their geodynamic environment of formation (e.g., Coulton et al., 1995). The topic of this work is on ophiolitic nappes remaining near the surface, thus excluding the case of dismembered meta-ophiolitic sequences occasionally exposed in the internal zones of orogenic belts. In principle, serpentinization within an ophiolitic nappe may witness the successive stages of oceanic accretion, intra-oceanic subduction (the ophiolite lying in the upper plate, for instance in the fore-arc region), obduction, and post-obduction evolution. Post-obduction events may involve post-convergence extension and/or collisional orogeny.

The Peridotite Nappe of New Caledonia is one of the few ophiolites in the world to have escaped collision after obduction (e.g., Cluzel et al., 2012). In this case, deciphering early serpentinization events should be easier. Recent work has shown that the Peridotite Nappe hosts various types of serpentine (Lahondère and Maurizot, 2009; Ulrich, 2010; Lahondère et al., 2012). An intimate association between deformation and the occurrence of serpentines is recognized in these studies, however no attempt has been made so far to characterize this deformation. More generally, structural studies carried out on the ultramafic section of ophiolitic nappes usually focus on serpentine-free high grade fabrics (e.g., Boudier et al., 1988; Suhr and Cawood, 1993; Cook et al., 2000). Studies including an analysis of serpentine-bearing faults and shear zones are relatively rare (Bailey et al., 2000; Titus et al., 2002; Schemmann et al., 2007; Laó-Dávila and Anderson, 2009; Federico et al., 2014).

In New Caledonia, earlier studies concerned with the Peridotite Nappe have focused on i) the high temperature intra-oceanic stages of deformation within the nappe (Prinzhofer et al., 1980; Titus et al., 2011), ii) the obduction process, however based essentially on the analysis of the rock units underlying the nappe (e.g., Cluzel et al., 2001, 2012; Spandler et al., 2005; Lagabrielle et al., 2013) and iii) post-obduction brittle extension that shaped the island as a large horst (e.g., Lagabrielle et al., 2005; Chardon and Chevillotte, 2006). Furthermore, much attention has been put on the chemistry and mineralogy of thick lateritic profiles formed at the expense of the peridotites, which led to the development of worldclass nickel

78 mineralizations (e.g., Orloff, 1968; Trescases, 1975; Butt and Cluzel, 2013). In contrast, only
79 limited work has concerned serpentines-bearing faults and shear zones that are ubiquitous
80 throughout the Peridotite Nappe, despite the common statement that the distribution of nickel
81 ore is highly dependent on this fault network (Leguéré, 1976; Cluzel and Vigier, 2008).

82 In this study, we had access to a recently opened large mining site in the Koniambo
83 Massif, one of the klippes of the Peridotite Nappe in northwestern New Caledonia (Fig. 1).
84 This site provides a quasi-continuous exposure of fresh rocks from the base of the nappe, near
85 sea level, up to ~800 m elevation, where the main laterite capping the peridotites occurs. We
86 focused on the study of structures and deformation associated with serpentines. These data
87 enable to describe the internal deformation of the nappe in relation with successive
88 serpentinization events. The implications of this study for the tectonic evolution of New
89 Caledonia are not discussed here and will be the topic of a distinct paper.

90 **2. Geological setting**

91 New Caledonia is located in the southwest Pacific Ocean, 1300 km east of Australia (Fig. 1).
92 On the main island, known as the "Grande Terre", the Peridotite Nappe overlies, with a sub-
93 horizontal tectonic contact (Avias, 1967; Guillon, 1975), a substratum composed of several
94 volcano-sedimentary units (Paris, 1981; Cluzel et al., 2001, 2012). The Peridotite Nappe is
95 essentially exposed in the "Massif du Sud", covering much of the southeastern third of the
96 Grande Terre, and as a series of klippes along the northwestern coast (Fig. 1). In the Massif
97 du Sud, the thickness of the nappe is at least 1.5 km and may reach 3.5 km (Guillon, 1975).
98 The nappe is mostly composed of harzburgites except in the northernmost klippes where
99 lherzolites dominate (e.g., Ulrich et al., 2010). Compositional layering is essentially
100 represented by 1 to 100 m-thick layers of dunite within the harzburgites. In the main part of
101 the nappe, the degree of serpentinization of the peridotites is variable but moderate (Orloff,
102 1968), serpentines occurring preferentially along a network of mm- to ~10 cm-thick fractures

and shear zones (e.g., Leguéré, 1976; Lahondère and Maurizot, 2009; Lahondère et al., 2012). Fracture infillings and veins with various textures are described, containing lizardite±chrysotile or antigorite±chrysotile and/or an additional type of light-coloured serpentine not firmly identified (Lahondère and Maurizot, 2009; Lahondère et al., 2012). Serpentinization becomes pervasive along the base of the nappe, forming a 'sole' in which deformation has been intense (Avias, 1967; Orloff, 1968; Guillon, 1975; Leguéré, 1976; Cluzel et al., 2012; Quesnel et al., 2013). The thickness of this sole is a few tens of meters in the Massif du Sud but reaches a few hundred meters in the northwestern klippes (Guillon, 1975; Maurizot et al., 2002). According to Ulrich (2010), serpentinization of the sole involved three stages, firstly a pervasive development of lizardite, secondly the formation of antigorite within mm to cm-thick veins, finally the formation of chrysotile in local veinlet networks. In some of the veinlets, Ulrich (2010) also reports the partial replacement of chrysotile by polygonal serpentine. Recently, Ulrich et al. (2014) established that polygonal serpentine is more widespread in the sole than previously thought, forming light green serpentine veins associated with chrysotile veinlets.

Following their exposure to aerial conditions, the peridotites have been subject to intense weathering under dominantly warm and wet climatic conditions. This has led to the development of laterites up to ~30 m thick (e.g., Chevillotte et al., 2006). Leaching of the peridotites by downward infiltrating meteoric waters has resulted in a redistribution of elements, leading to high nickel concentrations at the base of the weathering profile, in the transition zone between coarse-grained saprolite and the bedrock (Orloff, 1968; Trescases, 1975; Leguéré, 1976; Paris, 1981). Some veins with nickel-rich mineralizations show evidence for a syn-tectonic emplacement (Cluzel and Vigier, 2008). Magnesite veins, which frequently occur along the serpentine sole of the Peridotite Nappe, represent another by-product of the leaching of the peridotites by meteoric fluids (Ulrich, 2010; Quesnel et al., 2013). Quesnel et al. (2013) showed that at least some of these veins have been emplaced

during pervasive shearing along the sole.

In the Koniambo Massif, the Peridotite Nappe is exposed from its base, near sea level, up to ~800 m elevation (Fig. 2a,b). Map relations (Carroué, 1972; Maurizot et al., 2002) show that the basal contact is subhorizontal around much of the massif but delineates a large open antiform in the west (Fig. 2b). At elevations above ~400 m, the nappe is capped by a highly dissected and partly reworked lateritic profile (Maurizot et al., 2002). At lower elevations, laterites of the westerly-inclined Kaféaté plateau probably belong to a younger planation surface (Latham, 1977; Chevillotte et al., 2006). The Koniambo Massif essentially consists of harzburgites with interlayers of dunite that define a crude compositional layering with a fairly regular ENE-WSW strike and a ~50º southward dip (Maurizot et al., 2002). With regard to the degree of serpentinization, Maurizot et al. (2002) distinguished three main rock types, namely (i) moderately serpentinized peridotites in which the primary compositional layering is preserved, (ii) highly serpentinized peridotites and (iii) massive serpentinites. The latter form the serpentine sole of the nappe, about 200 m thick. The highly serpentinized peridotites overlie the sole and form a distinct layer which, according to Maurizot et al. (2002), is ~200 m thick on the western flank of the massif but thins out further east (Fig. 2a,b). The moderately serpentinized peridotites occupy the higher part of the massif.

3. Methods

3.1. Strategy

Field work focused on fresh rock exposures provided by the last ~5 years of mining activity in the Koniambo Massif. The serpentine sole is well exposed in the Vavouto peninsula, especially along two cross-sections here named VA1 (700 m long, striking N082º, Fig. 2c) and VA2 (a composite section ~330 m long with a mean N-S strike). The VA2 section shows the basal contact of the nappe and its substratum made of basalts and minor cherts (Fig. 3a). Further east, the mine access road runs from the base of the nappe (height spot 65 m in Figure

2a) to the upper part of the massif; it provides good outcrops of the intermediate level of highly serpentinized peridotites. The moderately serpentinized peridotites are exposed at higher levels of the access road and in a series of currently exploited open pits. We carried out preliminary field observations and sampled rocks with various textures and fabrics (veins, fracture infillings, fault coatings, cleavage domains within shear zones). We determined the mineralogical content of the samples, which then served as references for macroscopic assessment of the mineralogy within specific structures during renewed field work and structural analysis.

3.2. Analytical methods

Reference samples have been characterized through a multi-technique approach including transmission electron microscopy, microprobe analysis (not presented here) and Raman spectroscopy. Raman spectroscopy measurements were carried out at the laboratory GéoRessources Nancy, France, using a Horiba Jobin-Yvon Labram HR800 spectrometer and a visible ionized argon laser source with a wavelength of 514 nm. The output power of the laser was 100 mW and measurements were performed using an Olympus lens of x50 to focus the laser beam onto an area 1µm in diameter. Spectra are the average of 6 to 10 acquisitions of 20 s each to optimize the signal/noise ratio. For serpentine identification, only one region of the Raman spectrum has been investigated, between 3520 cm^{-1} and 3870 cm^{-1} (Fig. 4). This region enables to characterize the hydroxyl groups which are the most discriminant for distinguishing the polymorphs of serpentine (Auzende et al., 2004; Schwartz et al., 2013; Ulrich et al., 2014).

For analyzing the deformation, we focused our attention on shear zones and fault planes. The kinematics of shear zones have been determined using the obliquity of cleavage with respect to the shear zone walls (Fig. 5e,f) and, occasionally, the occurrence of a set of oblique shear bands. For determining the kinematics of faults, the offset of pre-kinematic

markers or the presence of subsidiary Riedel shears has occasionally been used, however in most cases we favoured the use of accreted slickenfibers with a clear staircase geometry (Fig. 5a,b,c,d). The advantage of stepped slickenfibers is to provide a robust sense-of-slip indicator and to allow establishing which mineral or mineral assemblage was stable during a given fault slip event (Durney and Ramsay, 1973; see also, e.g., Twiss and Moores, 1992).

The bulk deformation of densely faulted areas has been assessed using the FaultKin software of Allmendinger et al. (2012). The basic tenets of this software, described by Marrett and Allmendinger (1990), are the same as those of the right-dihedra method (Angelier and Mechler, 1977; Angelier, 1994). It should be noticed that the approach used by Marrett and Allmendinger (1990) is intended to provide a qualitative description of the strain ellipsoid, not the stress ellipsoid. Several authors have argued that, in essence, the analysis of fault slip data informs more about strain than about stress (e.g., Twiss and Unruh, 1998; Tikoff and Wojtal, 1999; Gapais et al., 2000). According to Célérier et al. (2012), methods aiming at retrieving paleostresses may be more suited for separating distinct subsets (presumed to witness successive tectonic events) within a given fault slip dataset whereas methods aiming at retrieving strain (e.g., Marrett and Allmendinger, 1990) may be more suited for yielding an average estimate of strain within a rock volume. In our case, the mineralogy of slickenfibers, which is of two types, has provided an independent criterion for separating the fault slip data into two subsets, therefore the ‘strain’ approach seems more appropriate.

4. Results

4.1. Reference samples

We here describe three hand specimens that are representative of field cases where serpentine occurs in association with deformation. The two first specimens come from higher levels of the Koniambo Massif. The third sample comes from the Vavouto peninsula, within the serpentine sole.

The first sample includes a ~1 cm-thick vein of light olive green serpentine with a massive aspect (Fig. 4a). The vein has been active as a fault plane as indicated by fine striations underlined by black oxides along a surface parallel to its margin. The Raman spectrum of the vein material (analysis #1-1) shows two closely spaced main bands centered on ~3688 cm^{-1} and ~3694 cm^{-1}, which are diagnostic of polygonal serpentine (Auzende et al., 2004; Ulrich, 2010; Ulrich et al., 2014).

The second sample includes a ~1 cm-thick vein of platy-fibrous serpentine (Fig. 4b). Outside the vein, the host rock shows a Raman spectrum (#2-1) with two main bands centered on ~3688 cm^{-1} and ~3696 cm^{-1}, indicating the presence of polygonal serpentine. The vein itself is composite. Two insulated domains with diffuse boundaries are made of darker serpentine showing a Raman spectrum (#2-2) with two main bands centered on ~3672 cm^{-1} and ~3700 cm^{-1}, typical for antigorite. The main part of the vein appears as an heterogeneous stack of fibers. The Raman spectrum of analysis #2-3 in this domain shows a minor band centered on ~3671 cm^{-1}, attesting for the presence of antigorite. In addition, the main band centered on ~3698 cm^{-1} and the adjacent poorly developed band at ~3688 cm^{-1} indicate the presence of polygonal serpentine or/and chrysotile. Finally, the margin of the vein is underlined by small domains of homogeneous light green serpentine. Their staircase distribution indicates that they formed as the result of a fault slip event. The Raman spectrum of analysis #2-4 shows a main band centered on ~3697 cm^{-1} and an adjacent poorly developed band at ~3690 cm^{-1} which, again, points to the presence of polygonal serpentine or/and chrysotile. In that case, however, chrysotile is unlikely because the serpentine in this part of the vein is massive and does not display the habitus of well defined submillimetric fibers that is typical for chrysotile (Lahondère and Maurizot, 2009; Ulrich, 2010; Lahondère et al., 2012). The small domains of polygonal serpentine have well defined boundaries, which suggests that they formed later than the adjacent domain of darker antigorite did. Furthermore, the platy-fibrous nature of the main part of the vein is typical for antigorite (e.g.,

Lahondère et al., 2012), therefore the occasional intimate association of antigorite and polygonal serpentine, like in analysis #2-3, can be interpreted as the result of a partial pseudomorphosis of antigorite by fine-grained polygonal serpentine. Thus, the crystallization of polygonal serpentine appears to postdate that of antigorite.

The third sample consists of a fist-sized elongate clast taken from one of the major shear zones met along the VA1 section (Fig. 2c). The clast, which is made of pervasively serpentinized harzburgite with few orthopyroxene relics, is embedded in a film up to 0.5 cm thick of homogeneous pale green serpentine (Fig. 4c,d). The Raman spectrum (analysis #3-1) shows two closely spaced main bands centered on ~3691 cm^{-1} and ~3697 cm^{-1}, indicating that the film consists of polygonal serpentine.

4.2. Field determination of the serpentine polymorphs associated with deformation

Based on the characterization of the three above samples as well as other reference samples, we have established a number of macroscopic criteria for a field assessment of the mineralogy of fault zones and shear zones. Within fault zones, antigorite and polygonal serpentine are both able to build macroscopic slickenfibers with a clear staircase geometry. For distinguishing the two polymorphs, the main argument is textural. Antigorite has a well expressed platy-fibrous aspect (see also, e.g., Lahondère et al., 2012) with fibers frequently several centimeters long (Fig. 5a). In contrast, polygonal serpentine is massive, matte, and develops only short slickenfibers (Fig. 5b,c). A second argument is the fact that polygonal serpentine is pale green whereas antigorite is generally darker (Figs. 4b,c,d and 5a,b,c). However, in the saprolitic levels, weathering modifies the colours and polygonal serpentine tends to become olive green (Figs. 4a and 5c). In addition, some fault planes bear slickenfibers showing mixed properties, with a clear platy-fibrous nature but a pale green colour and a matte aspect (Fig. 5d). In that case, taking into account the likeliness of a pseudomorphic replacement of antigorite by polygonal serpentine, as in the second reference

sample above, we have assumed that the slickenfibers witness a syn-antigorite slip event.

Antigorite and polygonal serpentine are also involved in shear zones. There, antigorite forms distinct lamellae (Fig. 5e) whereas polygonal serpentine is more massive despite the development of a pronounced cleavage (Fig. 5f). Most of the shear zones we have observed involve polygonal serpentine. There is always a close spatial coincidence between the shear zone walls and the margins of the serpentine body (Fig. 5e,f). The fabric in each shear zone is pronounced and, in principle, shearing might post-date serpentinization. Nevertheless, would shearing occur under physical conditions outside the stability range of a primary serpentine, it is expected that a new serpentine polymorph would easily crystallize during the pervasive deformation. Hence, for shear zones with an homogeneous serpentine content, we assume that shearing and mineral growth were coeval.

Lizardite and chrysotile were also observed in the field, with features similar to those reported by Ulrich (2010) and Lahondère et al. (2012). Dark lizardite is widespread, present as a diffuse grain-scale network in the peridotites and as infillings of ~1 mm to ~5 cm-wide joints. It is also found on the margins of many of the faults and shear zones that involve antigorite or polygonal serpentine (Fig. 5c,e). However, lizardite itself only rarely bears striations and, in our experience, never builds macroscopic slickenfibers, therefore we made no attempt to characterize the deformation associated with lizardite. Chrysotile occurs as very thin fibers always oriented at right angle to the vein walls within $\leq$ 1 cm-thick veinlets. Dense networks of subparallel veinlets are locally observed. Such veins can be interpreted as tension gashes, therefore, in principle, they could provide some clue on the tectonic regime that prevailed during chrysotile growth. Alternatively, tension gashes may open in the absence of a significant tectonic contribution, for instance due to fracturing assisted by fluid pressure. For this reason, and because these thin veins represent very small amounts of strain, we ignored them during the analysis of deformation.

4.3. Structural analysis

We identified three structural levels, which correlate with the rock horizons identified by Maurizot et al. (2002) on the basis of the intensity of serpentinization (Fig. 2a,b).

4.3.1 Upper structural level

The Upper structural level coincides with the domain of moderately serpentinized peridotites at higher levels of the massif. A dense network of fractures, most of them dipping steeply, crosscut the peridotites (Fig. 6a). The spacing between adjacent macroscopic fractures is always less than ~2 m. In between fractures, the least serpentinized peridotites show 'mesh' textures (e.g., Rouméjon and Cannat, 2014) resulting from a partial replacement of olivine by lizardite along grain boundaries and grain-scale microfractures (Fig. 6b). On the outcrop scale, in addition to 'dry' joints, many fractures are filled with one or several types of serpentine. When present together with another serpentine polymorph, lizardite occupies the margins of the fracture (Fig. 5c). When occurring together, antigorite and polygonal serpentine occupy the core vs. the margins of the fracture, respectively. As discussed with the second reference sample in Section 4.1 (Fig. 4b), polygonal serpentine formed later.

In most veins involving fibrous polygonal serpentine or/and antigorite, the fibers lie at a very low angle to the vein walls, hence these veins can be interpreted as fault zones (e.g., Durney and Ramsay, 1973). A total of 125 such faults has been measured in a series of open pits covering a relatively small area on the top of the Koniambo Massif (Fig. 2a). The syn-polygonal serpentine vs. syn-antigorite nature of each fault displacement has been determined by assessing the mineralogy of associated slickenfibers (Fig. 5a,b,c,d) (see Section 4.2). As a result, two fault subsets have been defined, which compare well in terms of orientation but have distinct kinematics (Fig. 7a,b). The majority of the faults with dominantly dip-slip movement have a normal sense of slip when associated with antigorite vs. a reverse sense of slip when associated with polygonal serpentine. Fault slip analysis documents two strikingly

different strain ellipsoids (Fig. 7c,d). The syn-antigorite faults yield a highly constrictional ellipsoid, as illustrated by the value of 0.17 computed for the R ratio ($R=(\varepsilon_2-\varepsilon_3)/(\varepsilon_1-\varepsilon_3)$). Consequently, λ_1, the axis of maximum stretching, is the most accurately defined; it lies horizontally with a N102º trend (Fig. 7c). The axis of maximum shortening, λ_3, plunges steeply (64º) to the north-northeast. The syn-polygonal serpentine faults yield an ellipsoid in the flattening field (R=0.71). Consequently, λ_3 is the most accurately defined axis; it lies subhorizontally with a N144º trend, while λ_1 plunges shallowly in the N057º direction (Fig. 7d). Figure 8 illustrates the results of fault analysis on the scale of a pit ~200 m wide within the main area of investigation (Pit 208) and on an isolated site located 2 km further northwest (Bilboquet, see Figure 2a for location). Fault slip analysis on these sites yields results that fit closely with those deduced from the bulk dataset.

Further southwest and at lower elevation with respect to the open pits, the mine access road provides a large outcrop near the transition between the upper and intermediate structural levels (Roadsite '620 m' in Figure 2a). It shows fault planes with slickenfibers as well as shear zones a few centimeters thick (Fig. 5f), both involving polygonal serpentine. Fault slip analysis yields an ellipsoid in the flattening field (R=0.66), with λ_3 shallowly plunging southward (27º) along a N006º trend (Fig. 9). This is broadly consistent with the syn-polygonal serpentine strain field deduced from the open pits (Fig. 7d), though with a ~40º clockwise rotation in the direction of λ_3. This difference could reflect differential large-size block rotations post-dating the measured fault slip increments. However, in this area, dunitic interlayers retain the same ENE-WSW strike and ~50º southward dip as elsewhere in the Koniambo Massif (Maurizot et al., 2002), therefore this hypothesis is unlikely. Hence, the difference is more likely to reflect a modification of the strain field through space or time.

4.3.2 Intermediate structural level

In the Intermediate structural level, the degree of serpentinization is overall high but

laterally variable. The main part is similar to exposures of the Upper structural level, with a dense network of serpentine-bearing fractures. The distinctive feature of the Intermediate structural level is that this rock mass is crosscut by low-dipping shear zones a few meters thick, characterized by a pervasive development of light green polygonal serpentine (Fig. 10a). Two such shear zones (SZ1 and SZ2) occur at high levels of the Intermediate structural level (Fig. 2a). The NE-SW horizontal spacing between the two shear zones is ~450 m. Continuous rock exposure along the mine access road enables to note that no similar shear zone exists between SZ1 and SZ2. Both SZ1 and SZ2 involve polygonal serpentine with a closely spaced cleavage as well as magnesite (Fig. 10b,c,d,e). In the case of SZ1, striations have not been observed. The direction of shearing is assumed to lie at right angle to the intersection between the cleavage and shear planes located along the margins of the shear zone (Fig. 10b,c), along a ~N034º trend (Fig. 10f). In the case of SZ2, a major fault plane in the core of the shear zone bears striations with a N039º trend while the relationship between cleavage and shear bands suggests a ~N085º trend for the direction of shearing (Fig. 10e,f). Both shear zones have top-to-SW kinematics. SZ1 has the attitude of a reverse-slip shear zone (Fig. 10a,b,c,f) while SZ2 combines reverse and dextral displacements (Fig. 10e,f).

At lower elevations, the mine access road crosscuts a prominent SW-dipping fault zone involving a ~30 m-thick pinch of fine-grained sediments (Maurizot et al., 2002) (Fig. 11a). These sediments are originally part of either the ‘Poya terrane’ (Maurizot et al., 2002) or, more likely, the ‘Nepoui flysch’ (D. Cluzel, personal communication, 2012). As a result, they represent a fragment of the volcano-sedimentary series that immediately underlie the Peridotite Nappe (Cluzel et al., 2001). Hence, the fault zone likely roots slightly beneath the basal contact of the nappe, or along it if one takes into account the fact that sheets of serpentinite are frequently mixed with substratum rocks around several klippes of the nappe (e.g., Maurizot et al., 1985). Within the fault zone, the main fault superposes highly sheared serpentinites onto the sediments (Fig. 11a). Its orientation is N146º, 38ºSW and it bears

pronounced striations with a N072º trend (Fig. 11b). Along this contact and across a structural thickness of at least 75 m above it, shear sense criteria indicate a reverse-slip (top-to-ENE) displacement (Fig. 11c,d). This movement is consistent with the incorporation of rocks from the substratum into the fault zone, and with the probable offset of the roof of the serpentine sole across it (Fig. 2a,b). This top-to-ENE fault can be viewed as a conjugate shear with respect to the top-to-SW SZ1 and SZ2 shear zones.

4.3.3 Lower structural level (the serpentine sole)

The best exposures of the serpentine sole lie in the Vavouto peninsula (Figs. 2, 3, 12 and 13). Further east, the map contour of the basal contact of the nappe implies a culmination of this contact slightly northwest of the Tambounan Peak (Fig. 2a). As a result, the surface probably dips westward beneath the peninsula, with a slope of ~6-7º (Fig. 2b). The contact is exposed at the eastern margin of the peninsula, displaying ~E-W-trending open folds on a ~100 m scale (Fig. 3a).

The rocks along the sole are brecciated and/or foliated. Breccias are well developed along the VA1 section (Fig. 12a) and consist of clasts of serpentinized peridotite separated by serpentine joints (Fig. 4d). Many joints bear very fine striations (Fig. 4c). The striations have extremely variable orientations, which probably results from the complexity of clast displacements/rotations during brecciation. Major shear zones occur along the VA1 section (Fig. 2c), marked by a reduction in clast size (Figs. 12a and 13a). The shear zone boundaries are dominantly diffuse, but locally change to sharp. The width of the main shear zones ranges from ~2 to ~10 m. In the shear zones, the greater density of fault planes subparallel to their walls tends to produce elongate clasts that locally define a crude foliation (e.g., in the upper part of Figure 13b). In the core of some shear zones, the planar fabric is more pronounced and locally oblique to the shear zone walls. In cases where this oblique fabric had the appearance of a closely spaced cleavage, it helped to assess the kinematics of the shear zone. In most

cases, however, it is difficult to decide whether the fabric could alternatively represent a dense pattern of Riedel shears, hence implying the opposite sense of shear compared to that deduced from an oblique cleavage. As a result, the kinematics of individual shear zones and shear planes along the VA1 section has essentially been deduced from their effect (offset and drag folding) on pre-existing markers (Figs. 12b and 13b).

The largest part of the VA2 section consists of serpentinites with a pronounced planar fabric (Figs. 3a and 12c). On a 10 cm scale, this fabric is underlined by a disjunctive anastomosing cleavage (Fig. 13c). When present, clasts are isolated, hence the rock retains a matrix-supported texture (Fig. 12d). Generally, the clasts have an elongate and subangular to rounded shape with a consistent orientation throughout the rock (Fig. 12d). As a result, the rock has the typical appearance of a mylonite. Early compositional layering has been transposed into parallelism with the cleavage (Fig. 12c), attesting for very large strains. Under microscope, the fabric of the foliated serpentinites is irregularly distributed but locally pervasive (e.g., in the right part of Figure 13d). A component of ductile deformation is thus involved. The northern end of the VA2 section shows that the foliated serpentinites occur immediately above the basal contact of the nappe (Fig. 3a). The southern end of the section shows that they underlie the part of the sole dominated by breccias through a relatively sharp transition zone (Fig. 3b). Hence, the foliated serpentinites form a distinct layer of most intensely deformed rocks at the base of the serpentine sole, with a thickness of at least 20 m.

As illustrated by the third reference sample in Section 4.1 (Fig. 4c,d), our observations indicate that the major shear zones along the VA1 section involve pale green polygonal serpentine as the main syn-kinematic mineral phase (Figs. 12a and 13a,b). This also applies to the layer of foliated serpentinites of the VA2 section (Figs. 12c,d and 13c). Magnesite also occurs within this layer and along the VA1 section, in the form of irregularly distributed veins and local stockworks (Figs. 2c, 12c and 13a). Magnesite occurs in close association with

406 polygonal serpentine (Figs. 12c,d and 13a,b,c). Evidence of the syn-kinematic nature of the
407 magnesite veins is shown in Figure 13 (see also Quesnel et al., 2013). In the macroscopic
408 examples b and c, the veins are offset by local shear planes that contribute to the bulk
409 shearing deformation. In addition to the vein infilling habitus, elongate clusters of partly
410 coalescent millimetric to centimetric nodules of magnesite are occasionally found. Figure 13d
411 shows part of a pluricentimetric nodule under microscope. Its right margin is irregular, made
412 up of submillimetric nodules of cryptocrystalline magnesite. This geometry, which suggests
413 an unconstrained growth of magnesite, could be taken as an indication that magnesite has
414 formed in the absence of contemporaneous deformation, after the development of the shear
415 fabric visible in the host serpentinite. However, the upper margin of the nodule is straight and
416 coincides with one of the shear bands related to this fabric. The relations between the nodule
417 and the shear band, highlighted in the enlargement, are clearly more in line with the shear
418 band post-dating the nodule than with the opposite. Overall, the relations seen in Figure 13d
419 are consistent with magnesite having grown during shearing.

420 The asymmetric distribution of shear zones along the VA1 (Fig. 2c) and VA2 (Fig.
421 12c) sections documents non coaxial deformation across the serpentine sole. The exposure
422 surface being smooth along both sections, the orientation of the main shear zones is difficult
423 to evaluate. Nevertheless, a dozen shear planes of significant size (several meters) have been
424 measured along the VA1 section (Fig. 12e). Their mean orientation is N141º, 46º SW. This
425 suggests top-to-SW kinematics for the bulk shearing deformation. Top-to-SW shearing is
426 consistent with the orientation of steep planar magnesite veins in between the shear zones
427 (mean value N134º, 62ºSW), interpreted as tension gashes (Quesnel et al., 2013), and with the
428 orientation of folds developed at the expense of magnesite veins within the shear zones (Fig.
429 12e). Top-to-SW shearing is also consistent with the apparent top-to-west vs. top-to-south
430 sense of shear observed along the ~W-E-trending VA1 vs. ~N-S-trending VA2 section,
431 respectively. The orientation of the ellipsoid delineated by the large ovoid clast in the upper

left corner of Figure 3a also fits with this interpretation. Along the VA1 section, the major shear zones with an apparent top-to-west sense of shear have a mean apparent dip of 24.5º (Fig. 2c). Assuming that the mean strike of these shear zones is N141º (i.e. the same as for the meter-scale shear planes) and taking into account the N082º strike of the VA1 section, the mean true dip of the major shear zones can be estimated at ~28º. Taking into account the likely ~6-7º westward slope of the basal contact of the nappe beneath the Vavouto peninsula (Fig. 2b), the obliquity of the main shear zones with respect to the boundaries of the serpentine sole is probably around 22º. This obliquity is consistent with an interpretation of the shear zones as large C'-type shear bands (Berthé et al., 1979; Passchier and Trouw, 1996) developed during strong tangential shear across the serpentine sole. Smaller equivalent structures are visible in Figures 12c, 13b and 13c. Finally, it should be noted that flat-lying antithetic shear planes also occur in the eastern part of the VA1 section (Figs. 2c and 12b). In Figure 12b, they crosscut the main southwest-dipping shear fabric, however their relationship with one of the major shear zones suggests that they may have developed contemporaneously.

5. Discussion

5.1. The distribution of deformation in the Koniambo Massif

Figure 14 summarizes the results of our structural analysis while Figure 15 illustrates the possible relationships between the three structural levels identified in the Koniambo Massif.

The Upper structural level is characterized by a very dense network of fractures filled with one or several types of serpentine. Antigorite and polygonal serpentine commonly form slickenfibers along fault planes, which we used for analyzing fault slip data. The bulk deformation associated with antigorite-bearing faults is characterized by a highly constrictional ellipsoid with λ_1 lying horizontally along a N102º trend. The bulk deformation associated with polygonal serpentine-bearing faults is characterized by an ellipsoid in the flattening field with λ_3 lying subhorizontally along a N144º trend.

The Lower structural level coincides with the serpentine sole. As a rule in New Caledonia (e.g., Avias, 1967; Leguéré, 1976; Cluzel et al., 2012), the serpentine sole of the Koniambo Massif is intensely deformed. Breccias dominate while foliated serpentinites, interpreted as mylonitic rocks, form a distinct basal layer at least 20 m thick. The sole has experienced pervasive non-coaxial deformation with a top-to-SW sense of shear. Polygonal serpentine and magnesite are syn-kinematic phases with respect to this deformation. Along the VA1 section, major low-dipping shear zones are distributed with a ~100 m lengthscale (Fig. 2c). As described in Section 4.3.3, their mean obliquity with respect to the basal contact of the nappe is estimated at ~22º. We interpret these shear zones as C'-type shear bands developed within a thick zone of strong tangential shear that coincides with the serpentine sole (Figs. 14 and 15; see also Lahondère et al., 2012, their figure 115). In line with this interpretation, no equivalent shear zone is observed above the serpentine sole.

The Intermediate structural level is characterized by the presence of several meters-thick reverse-slip shear zones. Top-to-SW shear zones are synthetic to pervasive shearing along the serpentine sole and, likewise, involve polygonal serpentine and magnesite as syn-kinematic mineral phases. Therefore, although we had no opportunity to observe this contact in the field, we suppose that the shear zones root along the roof of the serpentine sole, the whole sole acting as a décollement (Fig. 14 and, in Figure 15, geometric relationship 'r1'). In Figure 15, the roof of the sole is schematically shown as a distinct fault; in reality, it is more likely to coincide with a zone across which the intensity of brecciation progressively diminishes. In addition, some shear zones may root at deeper level (Fig. 15, relationship 'r2'), for instance along the relatively sharp contact between the foliated serpentinites and the overlying serpentinite breccias (Fig. 3b) and/or along the basal contact of the nappe. This possibility is suggested by the presence of a relatively large top-to-SW reverse-slip shear zone at the northern end of the VA2 section (Fig. 3a) and by the characteristics of the fault zone of Figure 11 (see Section 4.3.2 and below).

The NE-SW horizontal spacing between two consecutive top-to-SW shear zones, SZ1 and SZ2, is ~450 m. This is slightly less than the thickness of the Upper structural level in the Koniambo Massif (Fig. 2b) and much less than the thickness of the Peridotite Nappe in the Massif du Sud (≥ 1.5 km). This narrow spacing suggests that at least some of the shear zones do not cross the nappe up to the surface but remain confined to the Intermediate structural level. In fact, although rock exposures are abundant in the open pits of the top of the Koniambo Massif, we have not observed any such shear zone in the Upper structural level. Based on this indirect evidence, it is here suggested that the shear zones may connect to another flat-lying décollement located along the roof of the Intermediate structural level (Fig. 15, relationship 'r3'). Like for the roof of the sole, this décollement might not coincide with a distinct fault but with a zone across which the reverse-slip displacement of the shear zones could be absorbed through diffuse faulting. In addition, a few major shear zones may ramp up to the surface (Fig. 15, relationship 'r4'). No such shear zone is observed in the Koniambo Massif but one likely exists in the northern part of the nearby Kopéto-Boulinda Massif (see Figure 1 for location). It is highlighted by a north-dipping serpentinite sheet about 200 m thick that emanates from the serpentine sole of this massif, at elevations around 200 m, and climbs among the peridotites up to an elevation of at least 500 m (Maurizot et al., 1985, their figure 4; Maurizot, 2007). The precise geometry and the kinematics of this probable shear zone remain to be documented.

Finally, top-to-NE shear zones also exist in the Koniambo Massif, as subsidiary structures in the serpentine sole and as conjugate shears with respect to the top-to-SW shear zones in the Intermediate structural level. Because it roots along or slightly beneath the base of the serpentine sole and likely offsets its roof (Fig. 2b), the reverse fault zone of Figure 11 is probably a relatively late feature with respect to pervasive top-to-SW shearing along the sole. The shear zone labelled 'r2', in Figure 15, would be an equivalent synthetic shear zone.

5.2. The temporal evolution of deformation

Our analysis documents major variations in the orientation of the principal strain axes. At least part of these variations reflect a temporal evolution (Fig. 14). This is the case within the Upper structural level, where fault slip data associated with antigorite and polygonal serpentine were collected in the same restricted area but yielded two strikingly different strain ellipsoids. Microstructural observations indicate that polygonal serpentine postdates antigorite (see Sections 4.1 and 4.3.1), in agreement with the time sequence identified by Ulrich (2010) in the serpentine sole of the Koniambo Massif. Hence, the Upper structural level keeps the record of a temporal change from WNW-ESE horizontal stretching, during antigorite crystallization, to NW-SE horizontal shortening, during polygonal serpentine crystallization.

The origin of the other variations in orientation of the principal strain axes is more difficult to assess because they involve the same serpentine polymorph (polygonal serpentine) and occur across distinct levels of the nappe. Therefore, the change from NW-SE shortening in the Upper structural level to NE-SW shearing in the serpentine sole could reflect a spatial rather than a temporal evolution, i.e. vertical strain partitioning at a specific evolutionary stage of the nappe. The ~N-S direction of shortening recorded at an intermediate structural height, on roadsite ‘620 m’, may support this view. Nevertheless, the observed changes in shortening direction are more likely to reflect a temporal evolution. A first reason is that it seems difficult to conceive a tectonic setting in which the nappe would undergo horizontal shortening at right angle to its direction of displacement (assuming the latter is given by the direction of shear along the basal décollement). A second reason is the fact that, in the Intermediate structural level, the main shear zones, which accommodate NE-SW shortening, crosscut rocks with the same dense network of fractures as in the Upper structural level (Fig. 10a). This relation suggests that the event having produced NE-SW shortening in the Intermediate structural level (and top-to-SW shearing in the sole) is younger than the fracture

sets of the Upper structural level.

Thus, we suspect that both the syn-antigorite and the syn-polygonal serpentine fault sets identifed in the Upper structural level are older than the top-to-SW shear deformation observed in the serpentine sole. This contrasts with the opinion of Leguéré (1976) who supposed that the various sets of fractures he identified in the main mass of the nappe are all younger than the deformation recorded by the sole. According to Leguéré (1976), these fracture sets provide evidence for a three-step temporal evolution involving an episode of ENE-WSW compression, then an episode of NNW-SSE compression, then an episode of NNW-SSE extension. This scenario applies to the Kopéto-Boulinda and Koniambo Massifs, but the same events and the same chronology, with some variations in the orientation of the strain axes, are given by Leguéré (1976) for the other klippes of the Peridotite Nappe he examined, spread over the Grande Terre. The episode of NNW-SSE compression, of fairly constant orientation across the Grande Terre (Leguéré, 1976), correlates well with the syn-polygonal serpentine event we identified in the Upper structural level of the Koniambo Massif. The episode of NNW-SSE extension, which is more variable in orientation on the scale of the Grande Terre (extension is locally WNW-ESE to W-E, cf. Leguéré, 1976), may correlate with the syn-antigorite event we identified. Finally, the episode of ENE-WSW compression, locally modified to a NE-SW compression (Leguéré, 1976), correlates with the syn-polygonal serpentine±magnesite event we identified in the Intermediate structural level and the serpentine sole. If so, however, the chronology of events proposed by Leguéré (1976) differs strikingly from ours: his first event is our last one, and his last event is our first one. We ignore the reasons for this disagreement, but note that Leguéré (1976) did not provide details on the arguments he used for establishing his chronology. Our chronology is essentially based on the identification of a sequence of minerals associated with deformation, from antigorite to polygonal serpentine±magnesite. This sequence is consistent with a progressive lowering in temperature conditions (Ulrich, 2010), which may reflect a

559 modification of the geothermal gradient and/or the progressive reduction in thickness of the
560 nappe (Fig. 15). As a possible explanation for our disagreement with Leguéré (1976), we
561 might have failed to identify one or several late episodes of normal faulting that are reported
562 from the sedimentary series surrounding the klippes of the Peridotite Nappe (Lagabrielle et
563 al., 2005; Chardon and Chevillotte, 2006).

564 5.3. Relationships between deformation and serpentinization

565 The three structural levels identified in the Koniambo Massif show strikingly different styles
566 of deformation. These levels correlate fairly well with the subhorizontal lithological layering
567 of the massif defined by Maurizot et al. (2002), which refers to variations in the intensity of
568 serpentinization. Hence, it is tempting to consider that the intensity of serpentinization played
569 a major role in the way deformation has been distributed across the Peridotite Nappe. As
570 implicitly considered in several studies (e.g., Avias, 1967; Cluzel et al., 2001), the massive
571 serpentinites of the sole might represent a layer of soft rocks having led to the
572 individualization of a major décollement at the base of the nappe.

573 The Upper structural level displays a dense network of serpentine-bearing fractures,
574 many of which have been activated as faults. Nevertheless, the bulk deformation associated
575 with these faults is probably limited, as suggested by the fairly constant orientation of dunitic
576 interlayers all across the Upper structural level (Maurizot et al., 2002). Moreover, as
577 discussed in Section 5.2, the deformation recorded by the serpentine sole and the shear zones
578 of the Intermediate structural level is likely younger than most fault sets of the Upper
579 structural level. This supports the picture of an almost rigid Upper structural level by the time
580 shearing was accumulating along the sole (cf. the strain-depth diagram in Figure 15). Could
581 this behaviour relate to a least degree of bulk serpentinization in the Upper structural level?

582 Unlike in some parts of the Massif du Sud (e.g., Orloff, 1968), pristine peridotites are
583 virtually absent from the Koniambo Massif. The least serpentinized rocks are found in the

highest ~200 m of the massif. In the field, they are identified as they seem to retain a granoblastic texture, yet their dark green colour is symptomatic of a significant serpentine content. Under microscope, these samples show 'mesh' textures resulting from a partial replacement of olivine by lizardite (Fig. 6b). Serpentine mesh textures are essentially pseudomorphic, therefore peridotites with these textures usually preserve their pre-serpentinization fabrics (e.g., Wicks and Whittaker, 1977; Rouméjon and Cannat, 2014), which also applies in that case (Fig. 6b; for other examples from the Koniambo Massif, see Lahondère et al., 2012, their figures 301 to 304 and 309 to 312). This suggests that the Upper structural level behaved almost rigidly ever since the early development of lizardite.

The mesh texture in Figure 6b is classical (see also the examples of Lahondère et al., 2012) in the sense that lizardite forms connected 'mesh rims' surrounding isolated olivine 'mesh cores' (e.g., Rouméjon and Cannat, 2014). This is a key observation because theoretical considerations (e.g., Handy et al., 1999) as well as experimental results (Escartín et al., 2001) indicate that, with such a texture, the peridotite should be nearly as weak as pure serpentinite. The rock in Figure 6b contains ~25% serpentine (estimated from image analysis) whereas experimental evidence suggests that a ~10-15% serpentine content is enough for achieving the largest part of the strength drop with respect to the strength of a pure peridotite (Escartín et al., 2001). Therefore, it seems that the highly uneven vertical distribution of syn to post-serpentinization deformation across the height of the Koniambo Massif does not relate to a parallel gradient in rock strength: within the range of observed variations in the degree of serpentinization, all the rocks should have approximately the same strength (cf. Escartín et al., 2001).

5.4. What promoted strain localization at lower levels of the nappe ?

The above discussion has shown that the degree of serpentinization is probably not the factor which led deformation to localize along the sole of the nappe. A simple alternative may be

considered where the gradient in rock strength is not located within the Peridotite Nappe but arises from its juxtaposition against rocks of the substratum. In the Koniambo Massif, as for the other klippes of the northwestern coast, this substratum is essentially composed of basalts and dolerites (e.g., Guillon, 1975; Paris, 1981; Cluzel et al., 2001) (Fig. 3a). Such rocks are clearly stronger than serpentinites (e.g., Ildefonse et al., 2007) and, following Escartín et al. (2001), also stronger than slightly serpentinized peridotites. Hence, a strength profile may be conceived where the whole Peridotite Nappe is weak, overlying a stronger substratum. Deformation is then expected to concentrate in the part of the weak domain that is the closest to the strong one, i.e. on the soft side of the main rheological boundary. This could account for strain localization along the sole of the nappe.

Where basalts and dolerites underlie the Peridotite Nappe, the thickness of the serpentine sole is great (~100-200 m). This is the case in the Koniambo Massif and the other klippes of the northwestern coast (e.g., Guillon, 1975). In contrast, smaller klippes located further northeast, around the axis of the island, have a much thinner serpentine sole (~10-20 m) and a substratum made of pervasively schistose fine-grained sediments with a low grade metamorphic overprint. Typical examples are the Tchingou Massif (e.g., Maurizot et al., 1985) and a series of kilometer-sized klippes around the Ougne summit (Maurizot et al., 1989) (Fig. 1). Assuming that the thickness of the sole depends essentially on the intensity of shearing, and assuming that the total amount of shear, linked to the displacement of the nappe, is approximately constant over the area under consideration, this large difference in sole thickness is consistent with the hypothesis that a lower vs. higher amount of strain is accommodated by the nappe when its substratum is made of soft metasediments vs. strong mafic rocks, respectively. This supports our proposal that strain localization along the base of the nappe results from its juxtaposition against a stronger substratum.

6. Conclusion

Three structural levels have been identified in the Koniambo Massif. The Upper structural level, characterized by a dense network of fractures, keeps the record of at least two deformation events, the first associated with antigorite (WNW-ESE extension), the second with polygonal serpentine (NW-SE compression). The Lower structural level is represented by the serpentine sole. It consists of massive tectonic breccias overlying a layer of mylonitic serpentinites. The sole, which records pervasive tangential shear with top-to-SW kinematics, can be interpreted as a décollement at the base of the nappe. The Intermediate structural level exposes several meters-thick conjugate shear zones accommodating NE-SW shortening. Like the sole, these shear zones involve polygonal serpentine and magnesite as the main syn-kinematic mineral phases. The shear zones likely root into the basal décollement, either along its roof or, occasionally, around its base.

Even the least altered peridotites, in the Upper structural level, contain so much serpentine that, according to theoretical and experimental work, they should be nearly as weak as pure serpentinite. Hence, no strong vertical gradient in strength due to variations in the degree of serpentinization is expected within the exposed part of the nappe. Strain localization along the serpentine sole probably results from the juxtaposition of the nappe, made of weak serpentinized peridotites, against stronger mafic rocks. In line with this view, the serpentine sole is about ten times thinner when the substratum of the nappe is made of weak metasediments, compared to what it is when the substratum is made of basalts and dolerites.

Acknowledgments

GeoRessources contribution has been supported by ANR-10-LABX-21–LABEX RESSOURCES 21. This work benefited from fruitful discussions with Marc Ulrich, Dominique Cluzel and Pierre Maurizot. We gratefully thank Sarah J. Titus and an anonymous reviewer for their constructive comments, and Toru Takeshita for editorial handling.

References

Allmendinger, R.W., Cardozo, N., Fisher, D.M., 2012. Structural Geology Algorithms. Cambridge University Press, Cambridge, p. 289.

Angelier, J., 1994. Fault slip analysis and paleostress reconstruction. In: Hancock, P.L. (Ed.), Continental Deformation. Pergamon Press, Oxford, pp. 53-100.

Angelier, J., Mechler, P., 1977. Sur une méthode graphique de recherche des contraintes principales également utilisable en tectonique et en sismologie: la méthode des dièdres droits. Bull. Soc. Géol. France 19, 1309–1318.

Auzende, A.L., Daniel, I., Reynard, B., Lemaire, C., Guyot, F., 2004. High-pressure behaviour of serpentine minerals: a Raman spectroscopic study. Phys. Chem. Miner. 31, 269–277.

Avias, J., 1967. Overthrust structure of the main ultrabasic New Caledonian massives. Tectonophysics 4, 531–541.

Bailey, W.R., Holdsworth, R.E., Swarbrick, R.E., 2000. Kinematic history of a reactivated oceanic suture: the Mamonia Complex Suture Zone, SW Cyprus. J. Geol. Soc. London 157, 1107-1126.

Berthé, D., Choukroune, P., Gapais, D., 1979. Orientations préférentielles du quartz et orthogneissification progressive en régime cisaillant: l'exemple du cisaillement sud-armoricain. Bull. Minéral. 102, 265-272.

Boudier, F., Ceuleneer, G., Nicolas, A., 1988. Shear zones, thrusts and related magmatism in the Oman ophiolite: initiation of thrusting on an oceanic ridge. Tectonophysics 151, 275–296.

Butt, C.R.M., Cluzel, D., 2013. Nickel laterite ore deposits: weathered serpentinites. Elements 9, 123–128.

Carroué, J.P., 1972. Carte géologique de la Nouvelle-Calédonie à l'échelle 1/50000, feuille Pouembout. Bureau de Recherches Géologiques et Minières, map sheet and explanatory notes, p. 38.

686 Célérier, B., Etchecopar, A., Bergerat, F., Vergely, P., Arthaud, F., Laurent, P., 2012.
687 Inferring stress from faulting: from early concepts to inverse methods. Tectonophysics
688 581, 206–219.

689 Chardon, D., Chevillotte, V., 2006. Morphotectonic evolution of the New Caledonia ridge
690 (Pacific Southwest) from post-obduction tectonosedimentary record. Tectonophysics
691 420, 473–491.

692 Chevillotte, V., Chardon, D., Beauvais, A., Maurizot, P., Colin, F., 2006. Long-term tropical
693 morphogenesis of New Caledonia (Southwest Pacific): importance of positive epeirogeny
694 and climate change. Geomorphology 81, 361–375.

695 Cluzel, D., Aitchison, J.C., Picard, C., 2001. Tectonic accretion and underplating of mafic
696 terranes in the Late Eocene intraoceanic fore-arc of New Caledonia (Southwest Pacific):
697 geodynamic implications. Tectonophysics 340, 23–59.

698 Cluzel, D., Maurizot, P., Collot, J., Sevin, B., 2012. An outline of the geology of New
699 Caledonia; from Permian-Mesozoic Southeast Gondwanaland active margin to Cenozoic
700 obduction and supergene evolution. Episodes 35, 72–86.

701 Cluzel, D., Vigier, B., 2008. Syntectonic mobility of supergene nickel ores of New Caledonia
702 (Southwest Pacific). Evidence from faulted regolith and garnierite veins. Resource Geol.
703 58, 161–170.

704 Coleman, R., 1971. Plate tectonic emplacement of upper mantle peridotites along continental
705 edges. J. Geophys. Res. 76, 1212-1222.

706 Cook, C.A., Holdsworth, R.E., Styles, M.T., Pearce, J.A., 2000. Pre-emplacement structural
707 history recorded by mantle peridotites: an example from the Lizard Complex, SW
708 England. J. Geol. Soc. London 157, 1049–1064.

709 Coulton, A.J., Harper, G.D., O'Hanley, D.S., 1995. Oceanic versus emplacement age
710 serpentinization in the Josephine ophiolite: implications for the nature of the Moho at
711 intermediate and slow spreading ridges. J. Geophys. Res. 100, 22245-22260.

712 Dewey, J.F., Bird, J.M., 1971. Origin and emplacement of the ophiolite suite: Appalachian
713 ophiolites in Newfoundland. J. Geophys. Res. 76, 3179-3206.

714 Durney, D.W., Ramsay, J.G., 1973. Incremental strains measured by syntectonic crystal
715 growths. In: de Jong, K.A., Scholten, R. (Eds.), Gravity and Tectonics. Wiley, New
716 York, pp. 67–96.

717 Escartín, J., Hirth, G., Evans, B., 2001. Strength of slightly serpentinized peridotites:
718 implications for the tectonics of oceanic lithosphere. Geology 29, 1023–1026.

719 Federico, L., Crispini, L., Vigo, A., Capponi G., 2014. Unravelling polyphase brittle tectonics
720 through multi-software fault-slip analysis: the case of the Voltri Unit, Western Alps
721 (Italy). J. Struct. Geol. 68, 175-193.

722 Gapais, D., Cobbold, P.R., Bourgeois, O., Rouby, D., de Urreiztieta, M., 2000. Tectonic
723 significance of fault-slip data. J. Struct. Geol. 22, 881–888.

724 Guillon, J.H., 1975. Les massifs péridotitiques de Nouvelle-Calédonie. Mémoires de
725 l'Office de la Recherche Scientifique et Technique Outre-Mer, Paris, vol. 76, p. 120.

726 Handy, M.R., Wissing, S.B., Streit, L.E., 1999. Frictional-viscous flow in mylonite with
727 varied bimineralic composition and its effect on lithospheric strength. Tectonophysics
728 303, 175-191.

729 Hirth, G., Guillot, S., 2013. Rheology and tectonic significance of serpentinite. Elements 9,
730 107-113.

731 Ildefonse, B., Blackman, D.K., John, B.E., Ohara, Y., Miller, D.J., MacLeod, C.J., 2007.
732 Oceanic core complexes and crustal accretion at slow-spreading ridges. Geology 35, 623-
733 626.

734 Lagabrielle, Y., Chauvet, A., Ulrich, M., Guillot, S., 2013. Passive obduction and gravity-
735 driven emplacement of large ophiolitic sheets: the New Caledonia ophiolite (SW Pacific)
736 as a case study? Bull. Soc. Géol. France 184, 545–556.

737 Lagabrielle, Y., Maurizot, P., Lafoy, Y., Cabioch, G., Pelletier, B., Régnier, M., Wabete, I.,
738 Calmant, S., 2005. Post-Eocene extensional tectonics in Southern New Caledonia (SW
739 Pacific): insights from onshore fault analysis and offshore seismic data. Tectonophysics
740 403, 1–28.

741 Lahondère, D., Lesimple, S., Cagnard, F., Lahfid, A., Wille, G., Maurizot, P., 2012.
742 Serpentinisation et fibrogenèse dans les massifs de péridotite de Nouvelle-Calédonie.

743 Bureau de Recherches Géologiques et Minières, Public Report BRGM/RP-60192-FR, p.
744 458.

745 Lahondère, D., Maurizot, P., 2009. Typologie et protocole d'échantillonnage des occurrences
746 naturelles d'amiante en Nouvelle-Calédonie. Bureau de Recherches Géologiques et
747 Minières, Public Report BRGM/RP-57334-FR, p. 164.

748 Laó-Dávila, D.A., Anderson, T.H., 2009. Kinematic analysis of serpentinite structures and the
749 manifestation of transpression in southwestern Puerto Rico. J. Struct. Geol. 31, 1472-
750 1489.

751 Latham, M., 1977. On the geomorphology of northern and western New Caledonian
752 ultramafic massifs. In: International Symposium on Geodynamics in South-West Pacific,
753 27 August-2 September 1976, Noumea, New Caledonia. Editions Technip, Paris, pp.
754 235-244.

755 Leguéré, J., 1976. Des corrélations entre la tectonique cassante et l'altération supergène des
756 péridotites de Nouvelle-Calédonie. Ph.D. thesis, Université de Montpellier, France, p. 94.

757 Marrett, R., Allmendinger, R.W., 1990. Kinematic analysis of fault-slip data. J. Struct. Geol.
758 12, 973–986.

759 Maurizot, P., 2007. Cartographie d'aide à l'aménagement dans la zone Voh-Koné-
760 Pouembout-Poya. Phase 1: Mise à jour de la carte géologique sur les communes de Koné
761 et Pouembout et bilan des données existantes. Bureau de Recherches Géologiques et
762 Minières, Public Report BRGM/RP-54898-FR, p. 76.

763 Maurizot P., Eberlé J.M., Habault C., Tessarolo C., 1989. Carte géologique de la Nouvelle-
764 Calédonie à l'échelle 1/50000, feuille Pam-Ouégoa, 2^{e} édition. Bureau de Recherches
765 Géologiques et Minières, map sheet and explanatory notes, p. 81.

766 Maurizot, P., Feigner, D., Paris, J.P., 1985. Données nouvelles sur les « fils de serpentinite »
767 de Nouvelle-Calédonie. Géol. France 1, 61-67.

768 Maurizot, P., Lafoy, Y., Poupée, M., 2002. Cartographie des formations superficielles et des
769 aléas mouvements de terrain en Nouvelle-Calédonie, zone du Koniambo. Bureau de
770 Recherches Géologiques et Minières, Public Report BRGM/RP51624-FR, p. 45.

771 Maurizot, P., Vendé-Leclerc, M., 2009. Carte géologique de la Nouvelle-Calédonie à l'échelle

1/500000. Direction de l'Industrie, des Mines et de l'Energie – Service de Géologie de Nouvelle-Calédonie, Bureau de Recherches Géologiques et Minières.

Orloff, O., 1968. Etude géologique et géomorphologique des massifs d'ultrabasites compris entre Houailou et Canala (Nouvelle-Calédonie). Ph.D. thesis, Université de Montpellier, France, p. 189.

Paris, J.P., 1981. Géologie de la Nouvelle-Calédonie, un essai de synthèse. Mémoires du Bureau de Recherches Géologiques et Minières, vol. 113, p. 274.

Passchier, C.W., Trouw, R.A.J., 1996. Microtectonics. Springer, Berlin, p. 289.

Prinzhofer, A., Nicolas, A., Cassard, D., Moutte, J., Leblanc, M., Paris, J.P., Rabinovitch, M., 1980. Structures in the New Caledonia peridotites-gabbros: implications for oceanic mantle and crust. Tectonophysics 69, 85–112.

Quesnel, B., Gautier, P., Boulvais, P., Cathelineau, M., Maurizot, P., Cluzel, D., Ulrich, M., Guillot, S., Lesimple, S., Couteau, C., 2013. Syn-tectonic, meteoric water-derived carbonation of the New Caledonia peridotite nappe. Geology 41, 1063–1066.

Rouméjon, S., Cannat, M., 2014. Serpentinization of mantle-derived peridotites at mid-ocean ridges: mesh texture development in the context of tectonic exhumation. Geochem. Geophys. Geosyst. 15, 2354-2379.

Schemmann, K., Unruh, J.R., Moores, E.M., 2007. Kinematics of Franciscan Complex exhumation: new insights from the geology of Mount Diablo, California. Geol. Soc. Am. Bull. 120, 543-555.

Schwartz, S., Guillot, S., Reynard, B., Lafay, R., Debret, B., Nicollet, C., Lanari, P., Auzende, A.L., 2013. Pressure–temperature estimates of the lizardite/antigorite transition in high pressure serpentinites. Lithos 178, 197–210.

Spandler, C., Rubatto, D., Hermann, J., 2005. Late Cretaceous-Tertiary tectonics of the southwest Pacific: insights from U-Pb sensitive, high-resolution ion microprobe (SHRIMP) dating of eclogite facies rocks from New Caledonia. Tectonics 24, TC3003.

Suhr, G., Cawood, P.A., 1993. Structural history of ophiolite obduction, Bay of Islands, Newfoundland. Geol. Soc. Am. Bull. 105, 399–410.

Tikoff, B., Wojtal, S.F., 1999. Displacement control of geologic structures. J. Struct. Geol. 21, 959–967.

Titus, S.J., Fossen, H., Pedersen, R.B., Vigneresse, J.L., Tikoff, B., 2002. Pull-apart formation and strike-slip partitioning in an obliquely divergent setting, Leka Ophiolite, Norway. Tectonophysics 354, 101–119.

Titus, S.J., Maes, S.M., Benford, B., Ferré, E.C., Tikoff, B., 2011. Fabric development in the mantle section of a paleo-transform fault and its effect on ophiolite obduction, New Caledonia. Lithosphere 3, 221–244.

Trescases, J.J., 1975. L'évolution géochimique supergène des roches ultrabasiques en zone tropicale, formation des gisements nickélifères de Nouvelle-Calédonie. Mémoires de l'Office de la Recherche Scientifique et Technique Outre-Mer, Paris, vol. 78, p. 259.

Twiss, R.J., Moores, E.M., 1992. Structural Geology. W.H. Freeman and Company, New York, p. 532.

Twiss, R.J., Unruh, J.R., 1998. Analysis of fault slip inversions: do they constrain stress or strain rate? J. Geophys. Res. 103, 12205-12222.

Ulrich, M., 2010. Péridotites et serpentinites du complexe ophiolitique de la Nouvelle-Calédonie. Ph.D thesis, Université de Nouvelle-Calédonie et Université Joseph Fourier (Grenoble), France, p. 246.

Ulrich, M., Muñoz, M., Guillot, S., Cathelineau, M., Picard, C., Quesnel, B., Boulvais, P., Couteau, C., 2014. Dissolution–precipitation processes governing the carbonation and silicification of the serpentinite sole of the New Caledonia ophiolite. Contrib. Mineral. Petrol. 167, 952.

Ulrich, M., Picard, C., Guillot, S., Chauvel, C., Cluzel, D., Meffre, S., 2010. Multiple melting stages and refertilization as indicators for ridge to subduction formation: the New Caledonia ophiolite. Lithos 115, 223–236.

Wicks, F.J., Whittaker, E.J.W., 1977. Serpentine textures and serpentinization. Can. Mineral. 15, 459-488.

Figure captions

Fig. 1. Simplified geological map of the Grande Terre, New Caledonia, showing the exposures of ultramafic rocks. Most of these rocks are originally part of the Peridotite Nappe. Adapted from Maurizot and Vendé-Leclerc (2009).

Fig. 2. a) Geological map of the central and southern parts of the Koniambo Massif, adapted from Carroué (1972) and Maurizot et al. (2002). b) General cross-section of the Koniambo Massif, located in (a). c) Report of the main fault zones along the VA1 section, in the Vavouto peninsula.

Fig. 3. Two field views at the (a) northern and (b) southern ends of the VA2 section, in the Vavouto peninsula (location in Figure 2a).

Fig. 4. Close views of the (a) first, (b) second and (c & d) third reference samples discussed in the text, and corresponding Raman spectra.

Fig. 5. Field views of serpentine-bearing (a to d) fault planes and (e & f) shear zones in the Upper structural level.

Fig. 6. a) Field view of an open pit with a dense network of fractures, typical from the Upper structural level (location in Figure 2a). b) Photomicrograph of a sample representative of the least serpentinized peridotites within the Koniambo Massif, from the Upper structural level, in between the macroscopic fractures. The sample shows a typical ‘mesh’ texture composed of lizardite (Liz) mesh rims surrounding olivine (Ol) and orthopyroxene (Opx) mesh cores.

Fig. 7. Lower hemisphere, equal-area projection showing the orientation of all measured (a) syn-antigorite and (b) syn-polygonal serpentine faults at higher levels of the Koniambo Massif (location in Figure 2a), and (c & d) the result of the analysis of these fault slip data using the FaultKin software of Allmendinger et al. (2012). Kamb contours are shown for the axes of maximum stretching (in c) or maximum shortening (in d) with intervals in shades of grey as depicted in the legend. The parameter R equates $(\varepsilon_2-\varepsilon_3)/(\varepsilon_1-\varepsilon_3)$ and describes the

852 shape of the strain ellipsoid (R is 0 for pure constriction, 0.5 for plane strain, and 1.0 for pure
853 flattening). Nmax is the number of faults compatible with the computed ellipsoid.

854 Fig. 8. Lower hemisphere, equal-area projection showing the orientation of faults at two
855 specific sites (location in Figure 2a), and the result of the analysis of these fault slip data.

856 Fig. 9. Lower hemisphere, equal-area projection showing the orientation of faults and minor
857 shear zones at roadsite '620 m' (location in Figure 2a), and the result of the analysis of this
858 fault slip dataset. Kamb contours are shown for the axes of maximum shortening with
859 intervals in shades of grey as depicted in the legend.

860 Fig. 10. Field views of (a to d) SZ1 and (e) SZ2, two major low-dipping shear zones typical
861 from the Intermediate structural level (location in Figure 2a). Plg, polygonal serpentine; Mgs,
862 magnesite. f) Lower hemisphere, equal-area projection showing the orientation of structural
863 elements in the two shear zones (see the text).

864 Fig. 11. Field views of the reverse-slip fault zone with top-to-ENE kinematics shown in
865 Figure 2a,b.

866 Fig. 12. Field views of the serpentine sole in the Vavouto peninsula, along the (a & b) VA1
867 and (c & d) VA2 sections (location in Figure 2). Plg, polygonal serpentine; Mgs, magnesite.
868 e) Lower hemisphere, equal-area projection showing the orientation, along the VA1 section,
869 of large shear planes (shown as orange squares representing poles of planes), of planar
870 magnesite veins (shown as great circles) in between major shear zones, and of fold axes
871 (shown as black dots) of folded magnesite veins within the shear zones.

872 Fig. 13. Field views (a to c) and microphotograph (d) illustrating the relationships between
873 magnesite and deformation in the serpentine sole.

874 Fig. 14. Left, block-diagram depicting the style of deformation in the three structural levels
875 identified in the Koniambo Massif. For the Upper structural level, the drawing shows the

deformation associated with polygonal serpentine, rather than with antigorite, because polygonal serpentine is also the main mineral phase associated with major structures in the other structural levels. Roadsite '620 m' is shown at the top of the Intermediate structural level to highlight its location at lower elevation in comparison to the main area of fault measurements (see Figure 2a). Right, synthesis of the results of strain inversion as a function of the structural level (vertically) and as a function of the main minerals associated with deformation, which enable the determination of a sequence of events (horizontally).

Fig. 15. Schematic cross-section depicting the vertical distribution of deformation within the Peridotite Nappe by the time top-to-SW shearing occurred along the serpentine sole. 'r1' to 'r4' are geometric relationships discussed in the text. The thickness and the topography of the nappe are poorly constrained and are likely to have changed during deformation.

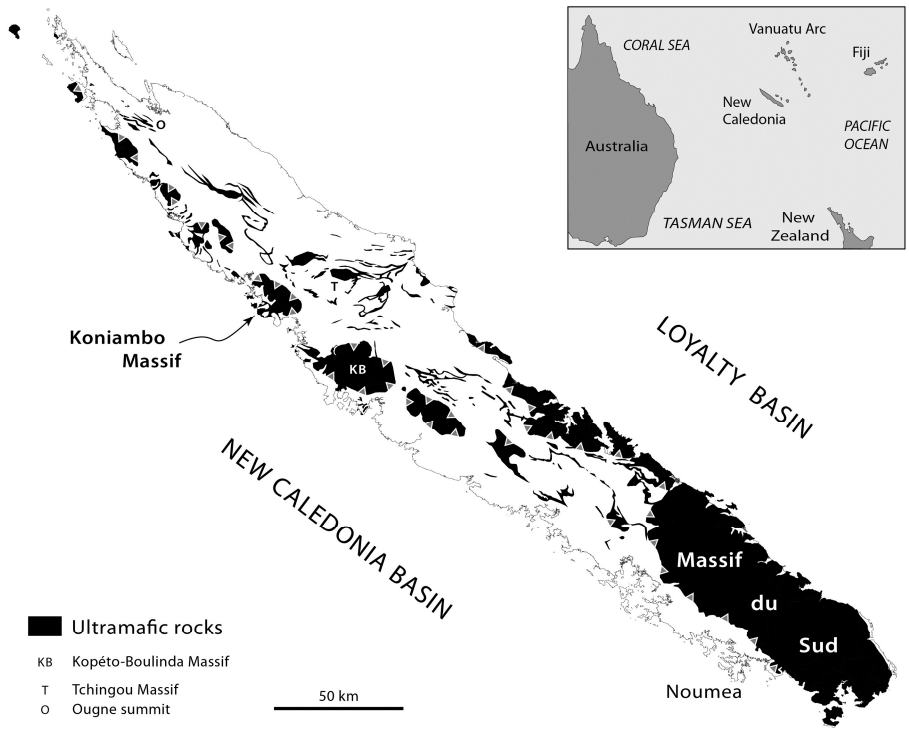

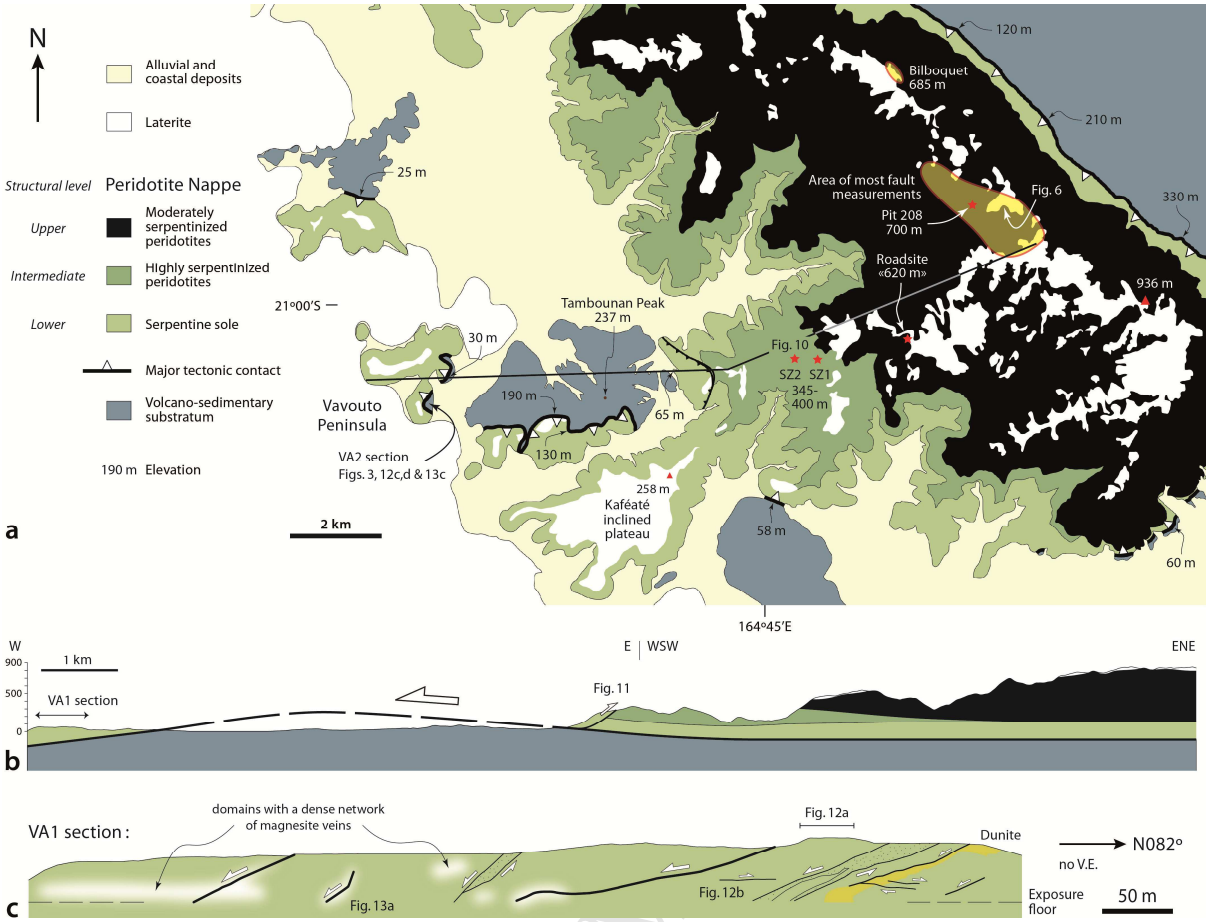

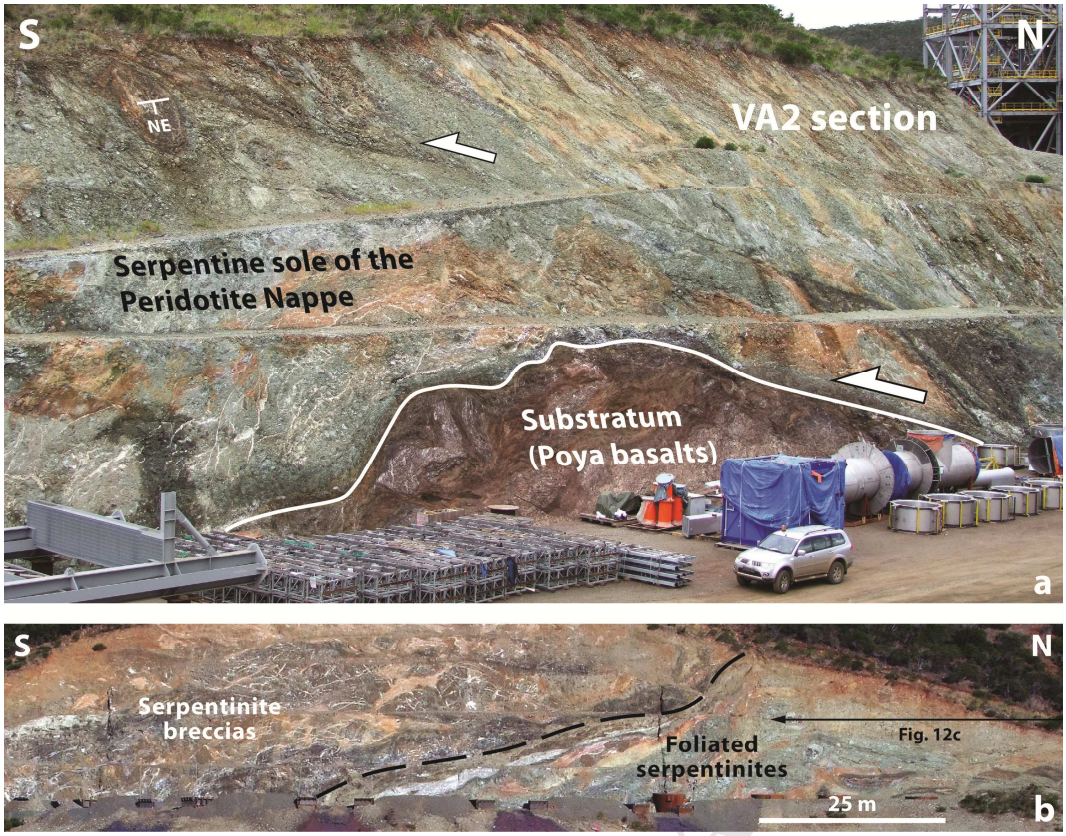

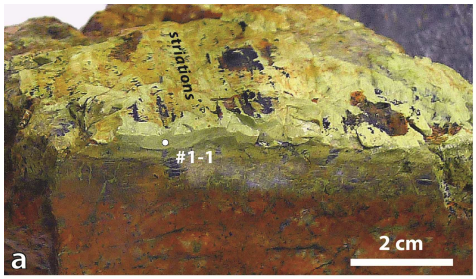

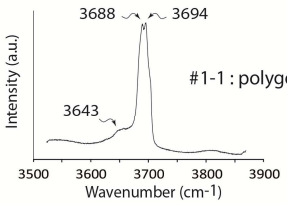

#1-1 : polygonal serpentine

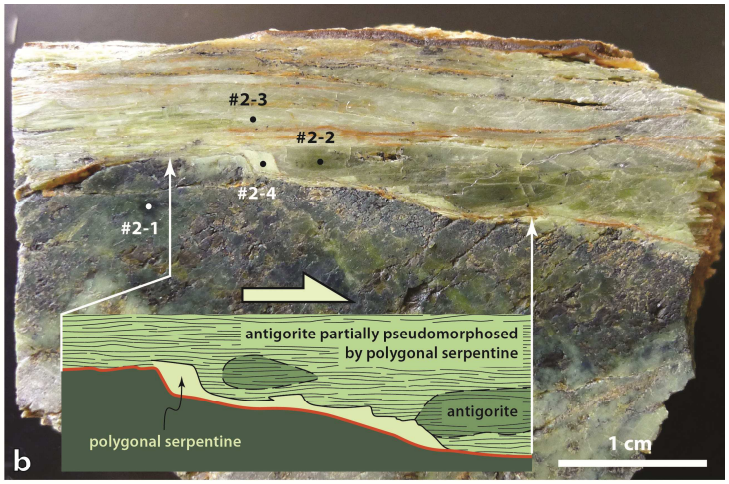

#2-1 : polygonal serpentine

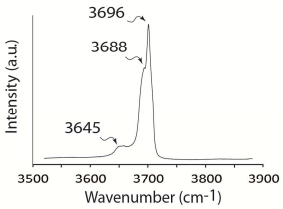

#2-2 : antigorite

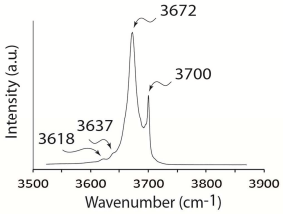

#2-3 : antigorite
+ polygonal serp. (± chrysotile ?)

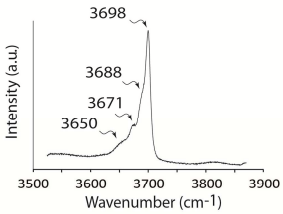

#2-4 : polygonal serpentine
(± chrysotile ?)

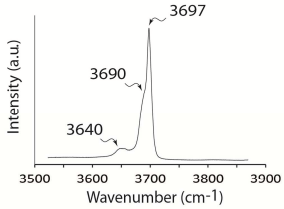

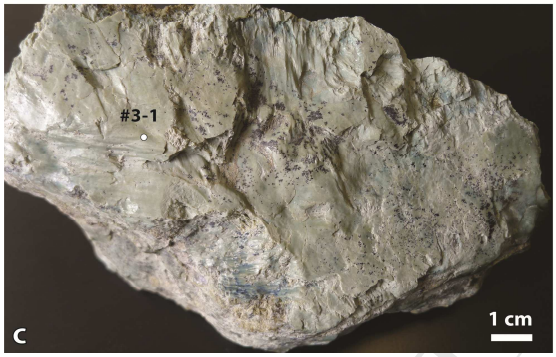

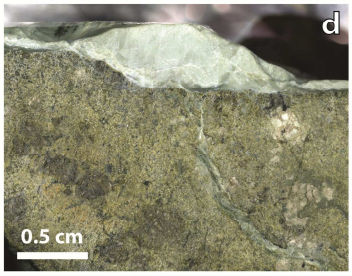

#3-1 : polygonal serpentine

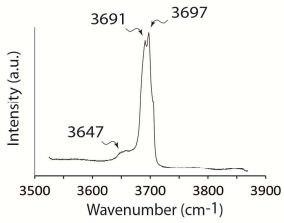

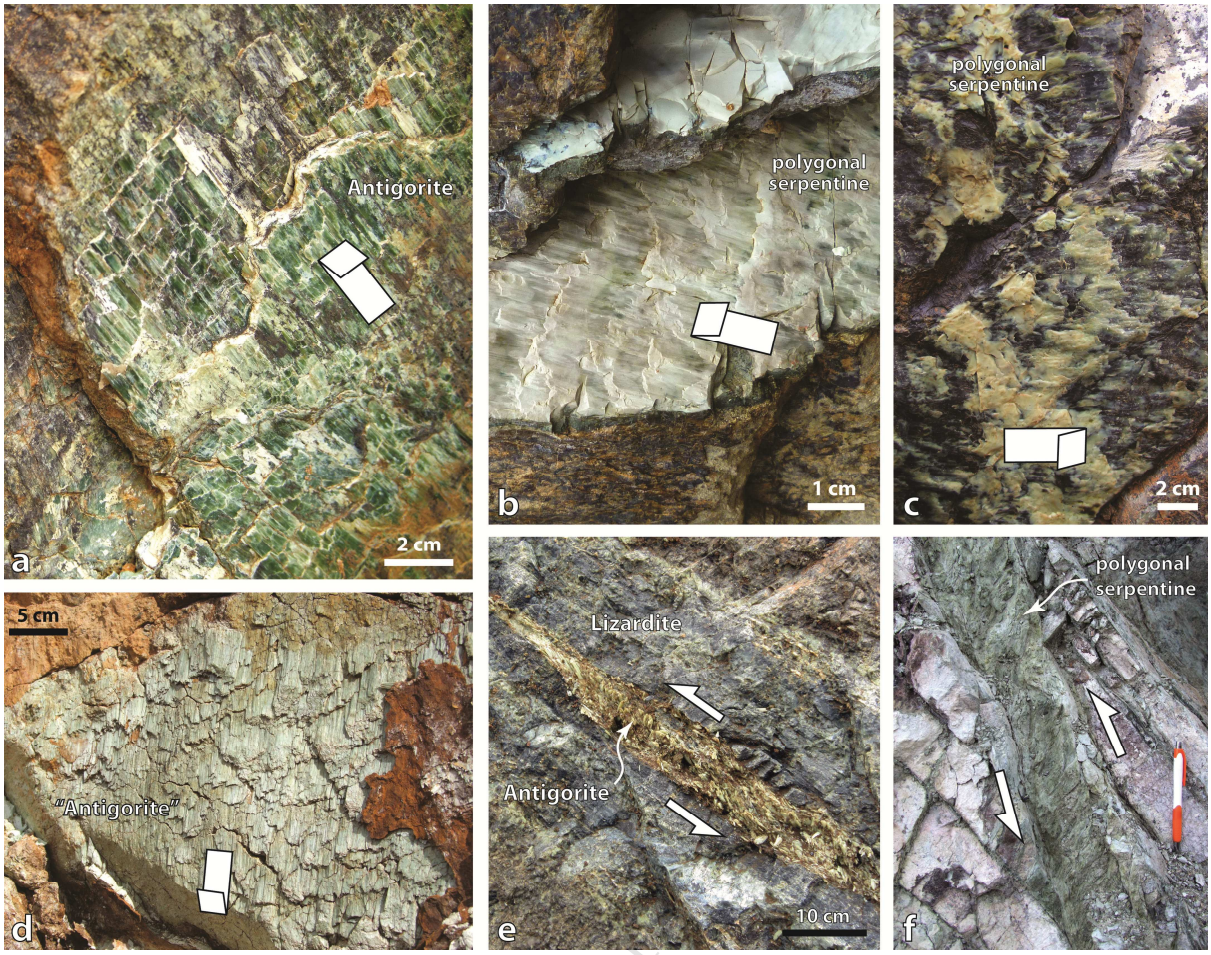

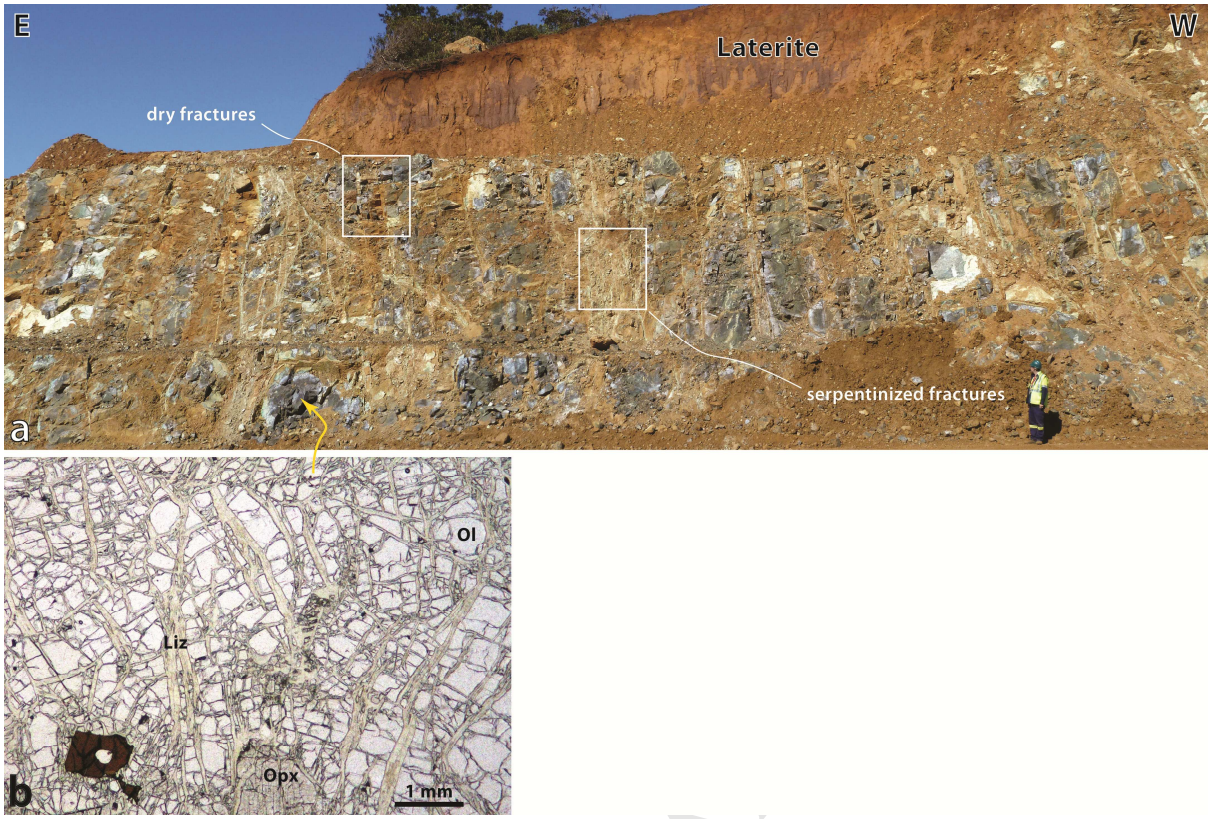
E
W
Laterite
dry fractures
serpentinized fractures
a

Ol
Liz
Opx
1 mm
b

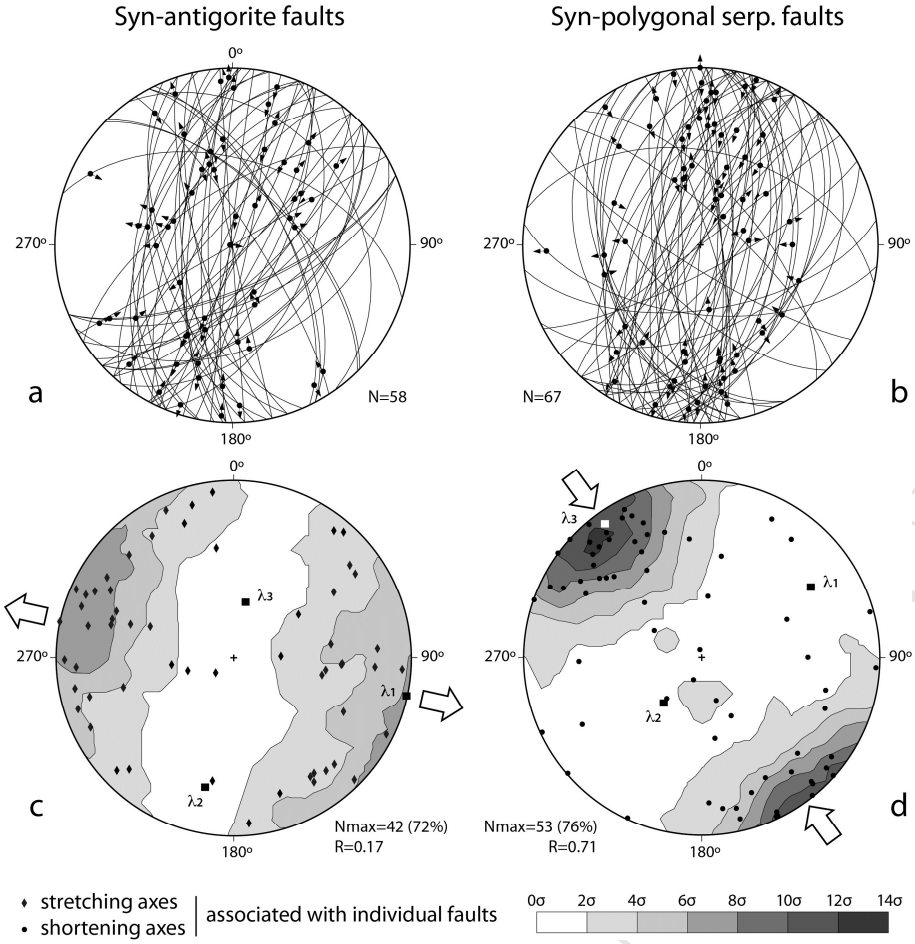

Syn-antigorite faults on Pit 208

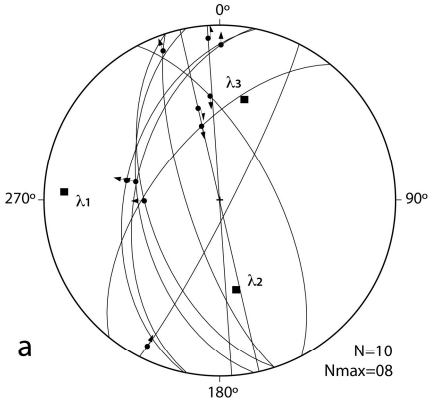

Syn-polygonal serp. faults on Pit 208

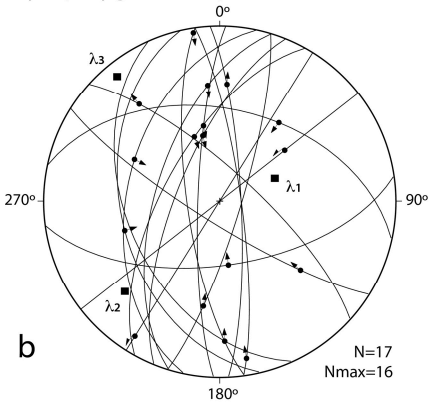

Syn-polygonal serp. faults on site «Bilboquet»

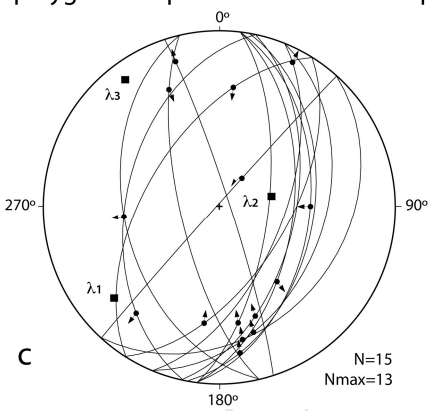

Syn-polygonal serpentine faults and minor shear zones, roadsite «620 m»

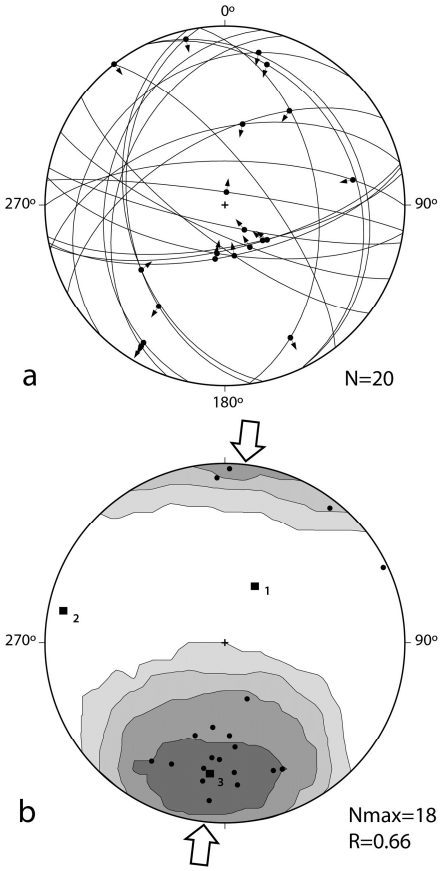

- shortening axes associated with individual faults

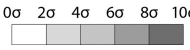

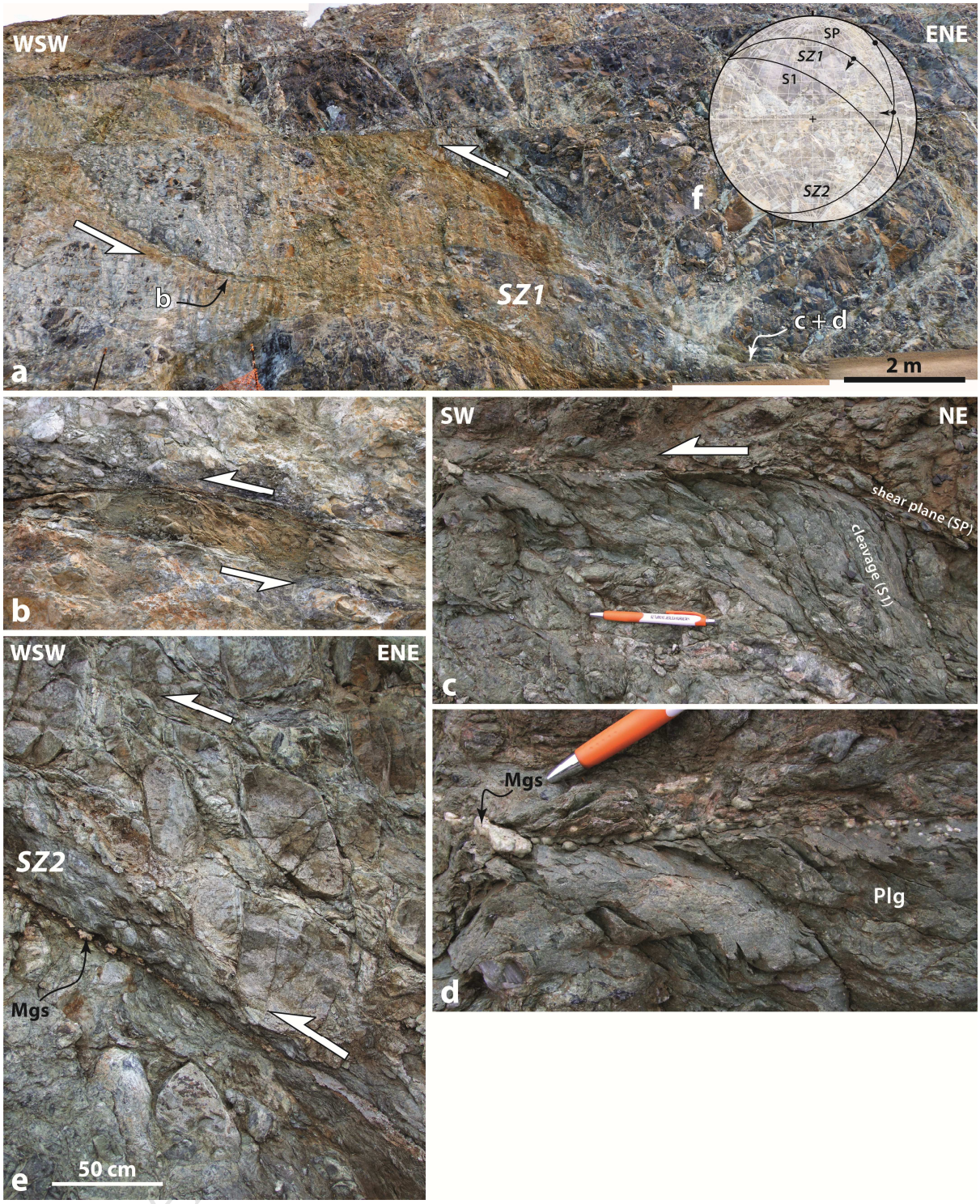
WSW
ENE
SP
SZ1
S1
SZ2
f
b
SZ1
c + d
2 m
a
b
SW
NE
shear plane (SP)
cleavage (S1)
c
WSW
ENE
SZ2
Mgs
50 cm
e
Mgs
Plg
d

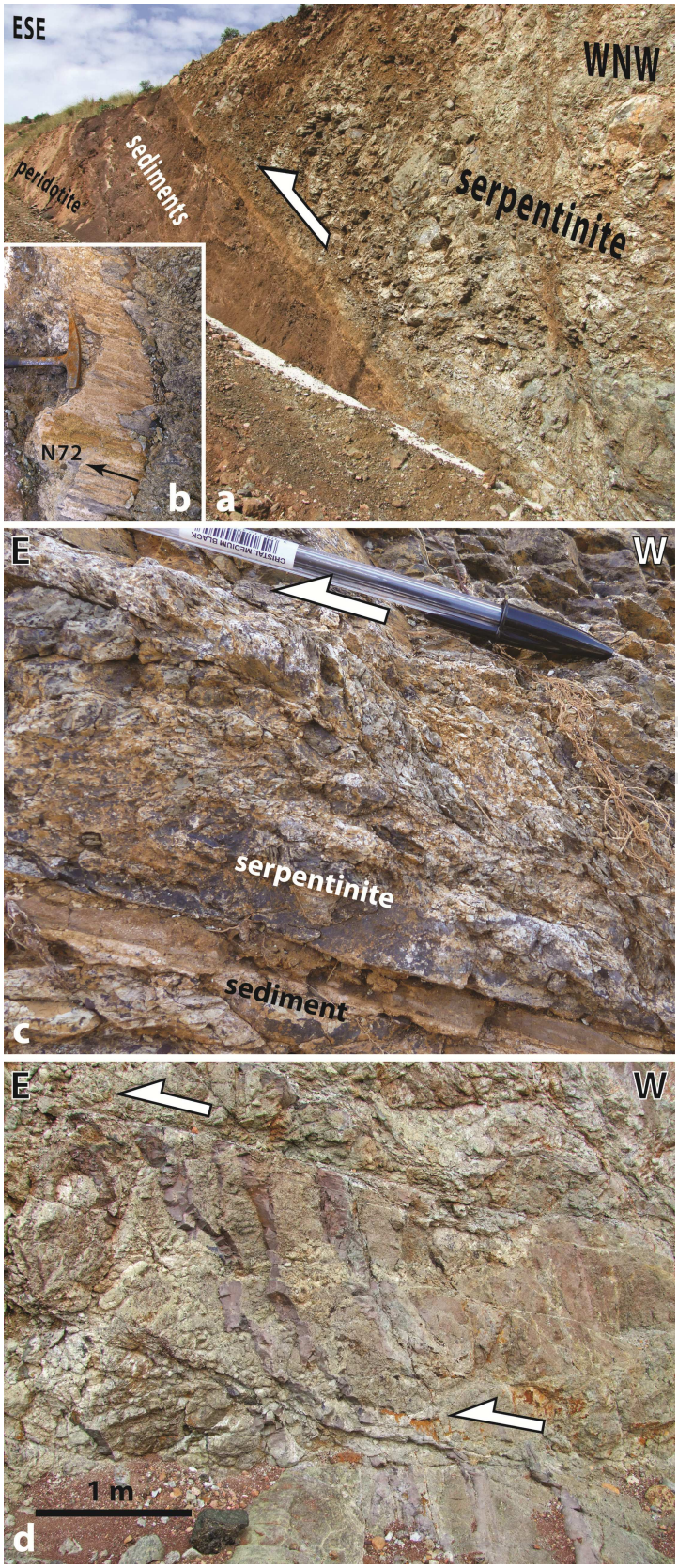

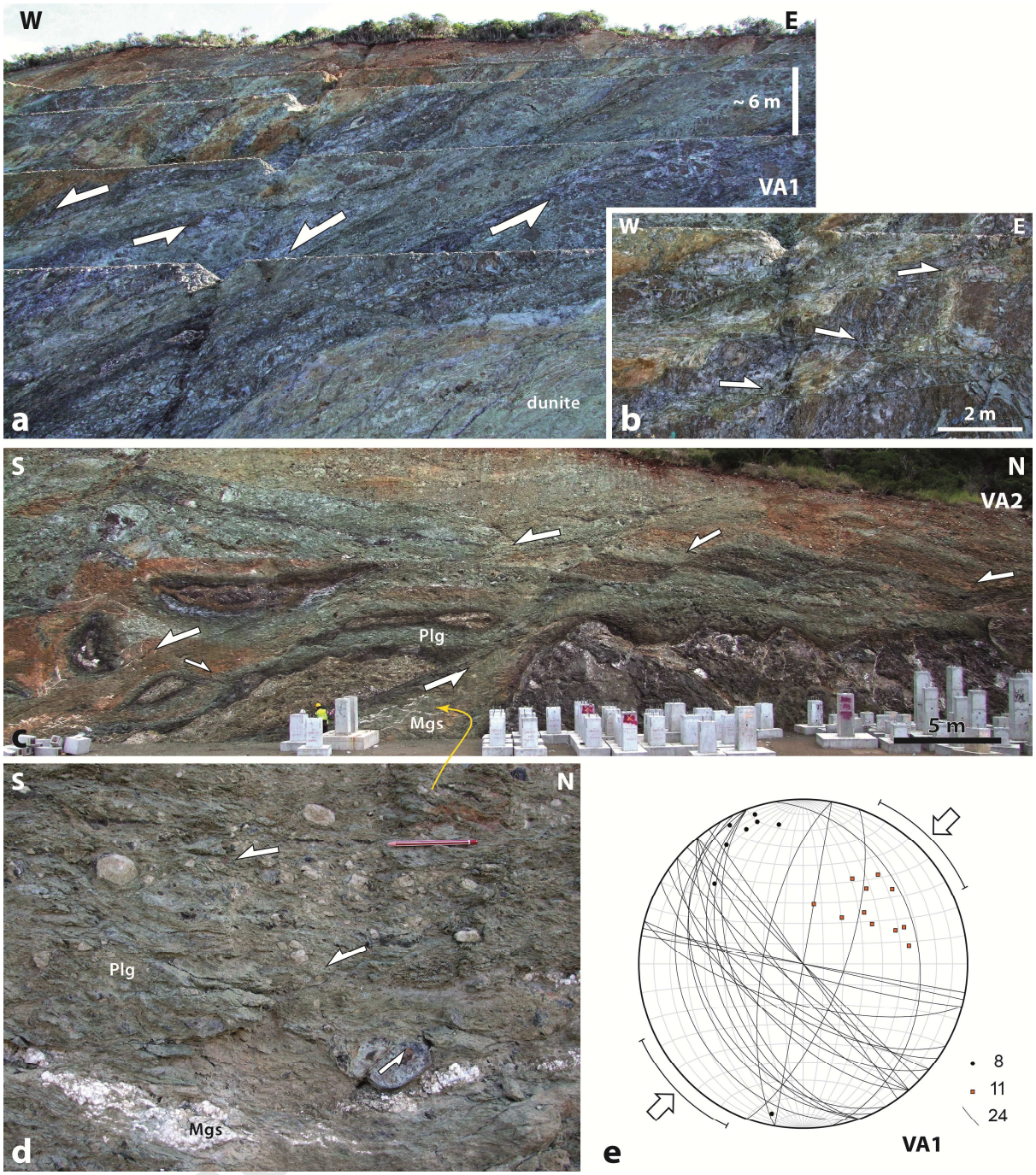
W
E
~ 6 m
VA1
dunite
a
W
E
b
2 m
S
N
VA2
Plg
Mgs
c
5 m
S
N
Plg
Mgs
d
e
8
11
24
VA1

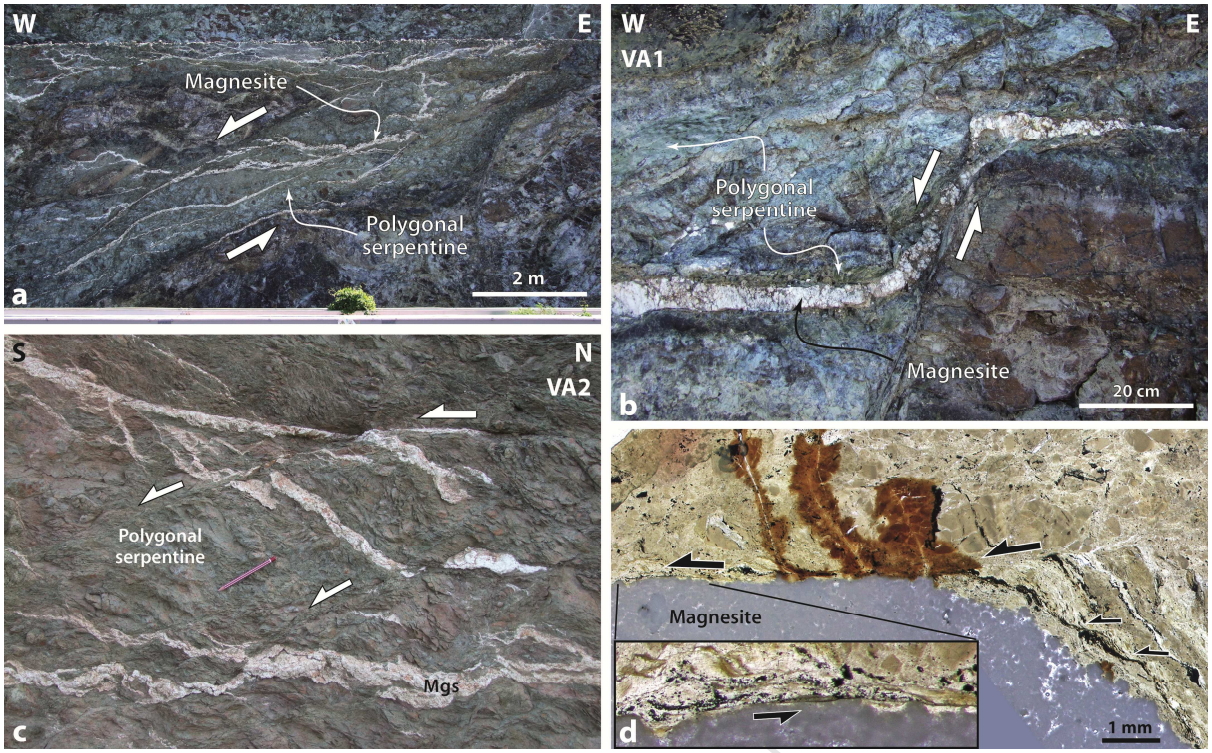

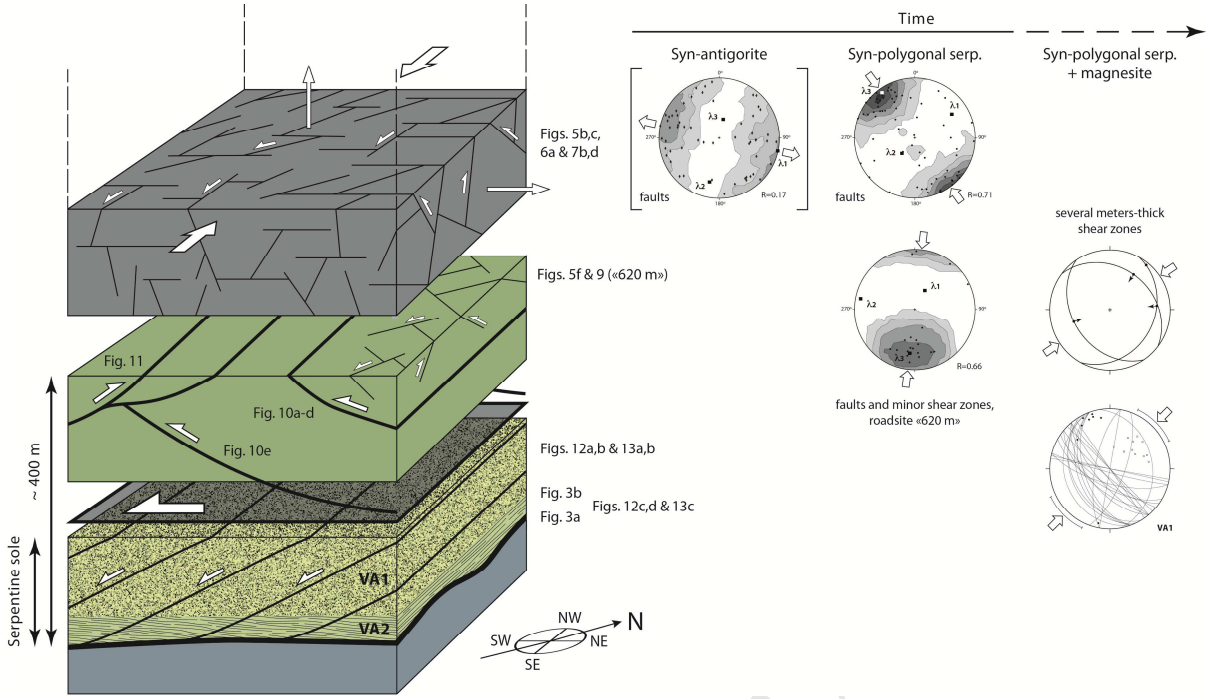

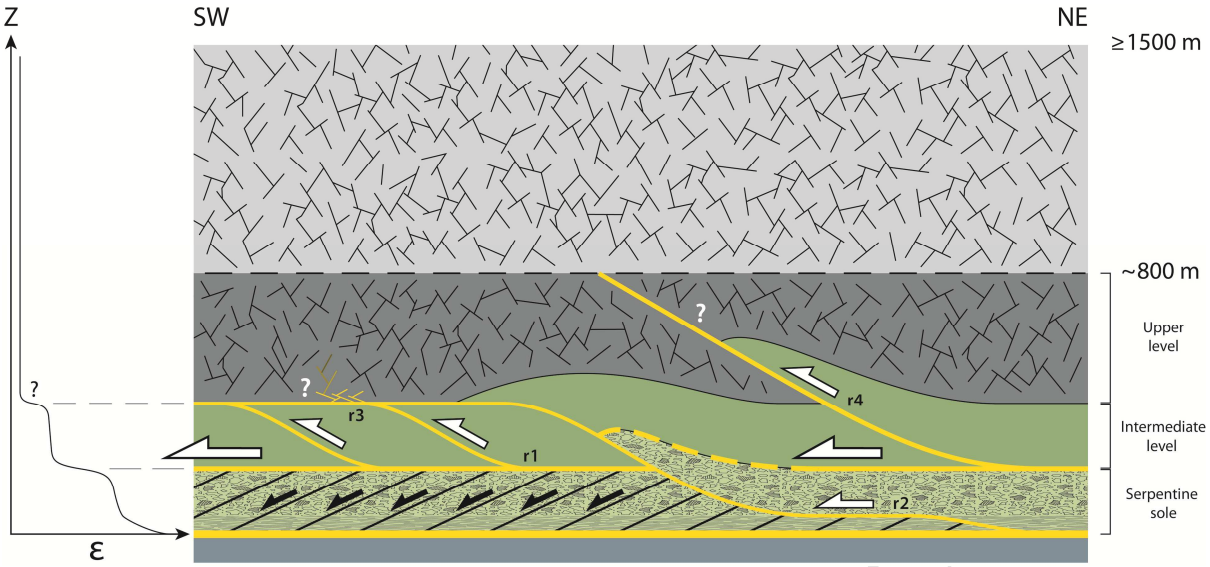

- We study the deformation associated with serpentines in the New Caledonia ophiolite
- Structural analysis is coupled with mineralogical characterization
- The evolution of deformation through space and time is described
- The reason for strain localization along the sole of the nappe is discussed